JAMES | Journal of Advances in Modeling Earth Systems

RESEARCH ARTICLE
10.1029/2022MS003046

Too Frequent and Too Light Arctic Snowfall With Incorrect Precipitation Phase Partitioning in the MIROC6 GCM

Yuki Imura[1,2] **and Takuro Michibata**[1,3]

[1]Department of Earth Sciences, Okayama University, Okayama, Japan, [2]Now at Atmosphere and Ocean Research Institute, The University of Tokyo, Kashiwa, Japan, [3]Graduate School of Natural Science and Technology, Okayama University, Okayama, Japan

Key Points:

- We examined seasonal model biases in precipitation types of Arctic clouds using a satellite simulator
- There are compensating errors between the cloud amount and snowfall, even for the prognostic precipitation scheme
- Realistic cloud and precipitation processes and their phase partitioning cannot be achieved by model tuning

Supporting Information:

Supporting Information may be found in the online version of this article.

Correspondence to:

T. Michibata,
tmichibata@okayama-u.ac.jp

Citation:

Imura, Y., & Michibata, T. (2022). Too frequent and too light Arctic snowfall with incorrect precipitation phase partitioning in the MIROC6 GCM. *Journal of Advances in Modeling Earth Systems*, *14*, e2022MS003046. https://doi.org/10.1029/2022MS003046

Received 13 FEB 2022
Accepted 26 OCT 2022

Abstract Cloud-phase partitioning has been studied in the context of cloud feedback and climate sensitivity; however, precipitation-phase partitioning also has a significant role in controlling the energy budget and sea ice extent. Although some global models have introduced a more sophisticated precipitation parameterization to reproduce realistic cloud and precipitation processes, the effects on the process representation of mixed- and ice-phase precipitation are poorly understood. Here, we evaluate how different precipitation modeling (i.e., diagnostic [DIAG] vs. prognostic [PROG] schemes) affects the simulated precipitation phase and occurrence frequency. Two versions of MIROC6 were used with the satellite simulator COSP2. Although the PROG scheme significantly improves the simulated cloud amount and snowfall rates, the phase partitioning, frequency, and intensity of precipitation with the PROG scheme are still biased, and are even worse than with the DIAG scheme. We found a "too frequent and too light" Arctic snowfall bias in the PROG, which cannot be eliminated by model tuning. The cloud-phase partitioning is also affected by the different approaches used to consider precipitation. The ratio of supercooled liquid water is underrepresented by switching from the DIAG to PROG scheme, because some snowflakes are regarded to be cloud ice. Given that the PROG precipitation retains more snow in the atmosphere, the underestimation becomes apparent when other models incorporate the PROG scheme. This depends on how much precipitation is within the clouds in the model. Our findings emphasize the importance of correctly reproducing the phase partitioning of cloud and precipitation, which ultimately affects the simulated climate sensitivity.

Plain Language Summary This study examined cloud and precipitation phase partitioning (i.e., the ratio between liquid and ice) in the Arctic using the MIROC6 global climate model (GCM). Despite recent advances in precipitation modeling by GCMs, the associations between the macrostructures (i.e., cloud coverage and precipitation rate) and phase partitioning have been little studied. Prognostic treatment of precipitation, which is a more sophisticated parameterization, yields seasonal and annual cloud cover and snowfall that are in better agreement with satellite observations. However, it tends to generate snowfall too frequently and too lightly, resulting in the misrepresentation of precipitation phase partitioning. In addition, there is a risk of overestimating the ratio of cloud ice to cloud liquid by including prognostic precipitation. The bias is difficult to remove by model tuning alone. If the models misrepresent the precipitation phase partitioning, then the bias will further influence feedback processes in a future warming scenario through the snow-to-rain phase change, similar to the cloud phase feedback. Our findings emphasize the importance of conducting process-oriented model evaluations on a regional scale.

1. Introduction

Cloud and precipitation processes that interact in a nonlinear manner with aerosols have an important role in Earth's energy budget, hydrological cycle, and climate feedbacks (e.g., Goosse et al., 2018; Hartmann & Short, 1980; Schär et al., 1999). However, the nature of these processes remains unclear and is difficult to represent due to their physical complexity and large spatiotemporal variations. The representation of cloud and precipitation phases is important in robustly reproducing feedbacks in a future climate scenario (Frey & Kay, 2018; Kay et al., 2018; Mülmenstädt et al., 2021).

Numerous studies have discussed cloud phase partitioning in mixed-phase clouds (e.g., Cesana et al., 2021; Ervens et al., 2011), given its influence on the radiative balance. This is because the radiative effects of liquid clouds and ice clouds at the same water content can differ significantly from each other, based on their macro- (i.e.,

altitude and temperature) and micro- (i.e., number concentration and droplet radius) physical properties (Hogan et al., 2003; Matus & L'Ecuyer, 2017). Despite the significance of the partitioning, many global climate models (GCMs) have underestimated the supercooled liquid fraction (SLF; Cesana et al., 2015; McCoy et al., 2016) until recently (Zelinka et al., 2020). Tan et al. (2016) showed that models with a lower SLF have higher potential for ice melting into liquid when the climate becomes warmer, which results in overestimation of a negative feedback that offsets climate warming (i.e., the cloud-phase feedback; Mitchell et al., 1989), due to a larger cooling effect caused by the reflection of shortwave radiation. The diversity of SLF values in GCMs is a major source of uncertainty in the cloud feedback mechanism and climate sensitivity.

In comparison with cloud phases, fewer studies have focused on the phase partitioning of precipitation (i.e., rain or snow), but this is also important in studies of climate change (Cohen et al., 2015; You et al., 2021). For example, snowfall increases downwelling longwave radiation at the surface (Li et al., 2019) and contributes to a warmer climate. Precipitation on sea ice can also have a major effect on the polar climate (e.g., Bintanja & Selten, 2014), given that snow accumulation promotes the growth of sea ice due to the high albedo of fresh snowfall, but also restricts it due to its insulating properties (Sturm et al., 2002), whereas rain decreases surface albedo and causes sea ice melting (Perovich et al., 2002). Given the important roles of precipitation, incorrect precipitation phase partitioning in GCMs would introduce biases into the simulated snow water equivalent, snow depth, and snow cover, as discussed by Jennings et al. (2018). As such, it is essential to correctly partition the precipitation phase for accurate climate modeling.

To evaluate partitioning, precipitation phase diagnostics utilizing a spaceborne active sensor are now available in GCMs with the aid of the satellite simulator COSP (Cloud Feedback Model Intercomparison Project Observational Simulator Package; Bodas-Salcedo et al., 2011), which enables a consistent comparison between satellite retrievals and GCM outputs. This approach was pioneered by Kay et al. (2018), who introduced the precipitation flag algorithm into the COSP version 2 (hereafter COSP2; Swales et al., 2018) in a manner that is consistent with the CloudSat observations and provides information on near-surface precipitation phases. Based on the near-surface precipitation frequency from the Community Earth System Model version 1 (CESM1), Kay et al. (2018) showed that CESM1 overestimates various types of precipitation frequencies on a global scale, except for the heavy rain category that is slightly underestimated. Lenaerts, Drew Camron, Wyburn-Powell, and Kay (2020) also found similar biases with CESM1 over the Greenland ice sheet. The results of these previous studies indicate that climate models do not robustly reproduce actual precipitation phase partitioning.

The discrepancy in precipitation frequency and phase partitioning can be partly attributed to the treatment of precipitation in GCMs. The Model for Interdisciplinary Research on Climate (MIROC) has adopted the diagnostic precipitation scheme (DIAG scheme; Ghan & Easter, 1992), which does not explicitly represent mixing ratios of precipitation, to reduce computational costs. This simplified DIAG scheme ignores the vertical sedimentation of precipitating hydrometeors across timesteps, which leads to further uncertainties in cloud and precipitation processes. As such, MIROC6 has recently introduced a prognostic precipitation scheme (PROG scheme; Michibata, Suzuki, Sekiguchi, & Takemura, 2019) that explicitly represents the mass and number mixing ratios of rain and snow along with their radiative effects. Recently, several models have introduced the PROG scheme, but the number of such models is still limited (e.g., Cesana et al., 2019; Forbes & Ahlgrimm, 2014; Gettelman et al., 2015; Rasch et al., 2019; Sant et al., 2015; D. N. Walters et al., 2011). The updated PROG scheme improves simulations including warm rain processes and the magnitude of aerosol-cloud interactions (e.g., Michibata & Suzuki, 2020; Michibata et al., 2020), similar to pioneering approaches used in other models (e.g., CAM5: Gettelman et al., 2015; ECHAM5–HAM: Sant et al., 2015). Both liquid-phase, and mixed- and ice-phase clouds have key roles in the global hydrological cycle (Mülmenstädt et al., 2015), and require further investigation in polar regions with the PROG scheme. For example, previous studies have reported that CAM6 incorporating the PROG scheme improves the occurrence frequency of Arctic liquid-containing clouds, which significantly affects the radiation budget (McIlhattan et al., 2020) and better represents cloud liquid and ice paths in the Arctic (Lenaerts, Gettelman, Van Tricht, van Kampenhout, 2020). Although other models have also incorporated an explicit precipitation scheme (e.g., E3SM: Rasch et al., 2019; GISS-E3: Cesana et al., 2019; ARPEGE-Climat 6.3: Roehrig et al., 2020; UM Global Atmosphere7: D. Walters et al. (2019); ECMWF-IFS: Forbes & Ahlgrimm, 2014), the effects of the PROG scheme on process representations in mixed- and ice-phase clouds are presently unclear. Therefore, a key question is how the PROG scheme changes the precipitation phase partitioning and its occurrence frequency.

Table 1
CloudSat Product and Variable Names Used in This Study

CloudSat product	Variable name
2B-GEOPROF	Radar_Reflectivity
2B-TAU	total_optical_depth, mean_effective_radius
2C-ICE	ice_water_path
2C-PRECIP-COLUMN	Precip_flag
2C-SNOW-PROFILE	snowfall_rate_sfc, snowfall_rate_sfc_uncert

In this study, we utilize the two versions of MIROC with the traditional DIAG scheme (Tatebe et al., 2019) and the latest PROG scheme (Michibata, Suzuki, Sekiguchi, et al., 2019). To examine the process-level model bias, our study uses multiple satellite data and a corresponding instrument simulator. In addition, we mainly focus on Arctic regions for the following reasons: (a) the Arctic climate becomes much warmer and wetter with climate warming (Boisvert & Stroeve, 2015; Screen & Simmonds, 2010; Serreze et al., 2009), and thus the reproducibility of either cloud or precipitation phase partitioning has large effects on the Arctic energy budget, sea ice extent, and climate predictions; (b) the estimate of a >50% increase in precipitation in Arctic regions by the end of the 21st century (Collins et al., 2013; Kattsov et al., 2007) emphasizes the importance of proper precipitation phase partitioning in GCMs when considering the Arctic; and (c) micro-physical processes within mixed- or solid-phase clouds that are ubiquitous in the Arctic have been little investigated with our model.

The remainder of this paper is organized as follows. Section 2 describes the satellite data sets and numerical model settings. Section 3 presents a comparison between the model simulations and satellite observations (i.e., COSP2). Finally, a summary and discussion are presented in Section 4.

2. Data and Methodology

2.1. Satellite Data

This study used multiple satellite data sets of the Afternoon Constellation (A-Train) to evaluate cloud and precipitation processes in the MIROC6 GCM. These sun-synchronous and polar-orbiting satellites nearly simultaneously observe the Earth, and fly approximately 705 km above the sea surface (Stephens et al., 2002). We used satellite data from: (a) the Cloud Profiling Radar (CloudSat CPR; Tanelli et al., 2008) (b) Cloud-Aerosol Lidar with Orthogonal Polarization (CALIPSO CALIOP; Winker et al., 2009) and (c) Moderate Resolution Imaging Spectroradiometer (Aqua MODIS; King et al., 1992).

2.1.1. CloudSat and MODIS Joint Product

CloudSat was launched by NASA in April 2006 for the purpose of resolving the vertical structure of cloud and precipitating hydrometeors. The CloudSat CPR is an active sensor operating in the W-band (94 GHz) with a minimum detectable cloud reflectivity of −28 dBZ. The footprint of the CPR is 1.4 km cross-track and 1.8 km along-track, and the vertical resolution is 480 m oversampled to 240 m (Stephens et al., 2008).

The Aqua satellite carries a passive MODIS sensor that observes emitted radiation in a range of channels from 0.41 to 14.5 μm. This multispectral sensor has a relatively fine spatial resolution of <1 km and a broad swath of 2,330 km. The CPR and MODIS observe the same location within a short time distance, and thus the combined use of the active and passive sensors provides us with more detailed insights into the process-level, aerosol-cloud-precipitation interactions (e.g., Kubar et al., 2009; Nakajima et al., 2010; Suzuki & Stephens, 2008).

The variables available from each CloudSat R04 product utilized in this study are summarized in Table 1. We used the 2B-GEOPROF product (Marchand et al., 2008) for the radar reflectivity profile; the 2B-TAU product (Polonsky et al., 2008) for the cloud optical depth and droplet effective radius from the 2.1 μm MODIS radiance channels (Ackerman et al., 1998); the 2C-ICE product (Deng et al., 2010) for the ice water path (IWP) from CPR and CALIOP; the 2C-PRECIP-COLUMN product (Haynes et al., 2009) for the near-surface precipitation incidence flag (i.e., the precipitation flag); and the 2C-SNOW-PROFILE product (Wood et al., 2013) for the snowfall rate at the surface and its uncertainty. The precipitation flag indicates various types of intensity and the phase of near-surface precipitation (Table 2; Section 2.3). This study used these data from January 2007 to December 2010, since CloudSat has operated only in the daytime since 2011 as a result of battery malfunction.

2.1.2. CALIPSO-GOCCP

CALIPSO was launched as part of the A-Train constellation and has operated since 2006 along with CloudSat. CALIOP carried on CALIPSO is a LiDAR that provides backscatter profiles at 532 and 1,064 nm, and collects information on the vertical structure of aerosols and clouds around Earth (Winker et al., 2013, 2009). This active

Table 2
Description of the Precipitation Flags Applied to COSP2[a]

Value for flag	Condition over the ocean	Condition over the land	Meaning
Flag indicating rain ($F_{ice} < 0.1$ over ocean; $T_{surf} > 275$ K over land)			
1	$-15 <$ dBZ < -7.5	$-15 <$ dBZ < 5 and $Z_{max} < 2.5$ dBZ	Rain possible
2	$-7.5 <$ dBZ < 0	$-15 <$ dBZ < 5 and $Z_{max} > 2.5$ dBZ	Rain probable
3	dBZ > 0	dBZ > 5 or $Z_{max} > 10$ dBZ and PIA > 30 dBZ	Rain certain
8	PIA > 40 dBZ	PIA > 40 dBZ	Heavy rain
Flag indicating mixed-phase ($0.1 < F_{ice} < 0.9$ over ocean; 273 K $< T_{surf} <$ 275 K over land)			
6	$-15 <$ dBZ < -5	$-15 <$ dBZ < -2.5 and $Z_{max} < -5$ dBZ	Mixed precipitation possible
7	dBZ > -5	dBZ > -2.5 or $Z_{max} > 10$ dBZ and PIA > 30 dBZ	Mixed precipitation certain
Flag indicating snow ($F_{ice} > 0.9$ over ocean; $T_{surf} < 273$ K over land)			
4	$-15 <$ dBZ < -5	$-15 <$ dBZ < -5	Snow possible
5	dBZ > -5	dBZ > -5	Snow certain
Others			
0	dBZ < -15	dBZ < -15	No precipitation
9			Uncertain

[a]Rain, mixed, and snow phases were classified based on the fraction of ice (F_{ice}) over the ocean and surface air temperature (T_{surf}) over the land. Near-surface unattenuated and attenuated radar reflectivity (dBZ) were used as the thresholds over the ocean and land, respectively. PIA is the two-way radar beam attenuation. Uncertainflag (9) was allocated if acquired conditions were not applied to any definition of flags 0–8.

sensor can detect high thin clouds that CloudSat CPR cannot observe due to its detection limitations (Mace & Zhang, 2014).

The GCM-Oriented CALIPSO Cloud Product (CALIPSO-GOCCP) is a data set designed for evaluating cloud properties simulated in GCMs by utilizing the same algorithm as the LiDAR simulator adopted in the COSP (Chepfer et al., 2010). CALIPSO-GOCCP uses the attenuated backscattered (ATB) profile at 532 nm embedded in the CALIPSO LiDAR Level 1 product (Winker et al., 2009). The original vertical resolution for the ATB profile is 30 m below 8.2 km, but is converted to 480 m to be consistent with the GCMs.

Pixels are defined as being cloudy if the value for the LiDAR scattering ratio acquired from the modified ATB profile is >5. The cloud fraction (CF) is then determined as the number of cloudy pixels (n) divided by the total number of observed pixels. The data are classified by pressure as low-level (>680 hPa), middle-level (440–680 hPa), and high-level (<440 hPa) clouds. Based on temperature, ATB, and cross-polarized ATB (ATB⊥), cloudy pixels are then categorized as liquid- or ice-phase (Cesana & Chepfer, 2013; Cesana et al., 2012). The liquid cloud fraction (CF_l) and ice cloud fraction (CF_i) are represented as follows:

$$CF_l = \frac{n_l}{n} \times CF \quad (1)$$

$$CF_i = \frac{n_i}{n} \times CF, \quad (2)$$

where n_l and n_i are the number of cloudy pixels defined as liquid and ice, respectively. The mixed-phase clouds are classified as either n_l or n_i, according to the ATB thresholds, as detailed by Cesana and Chepfer (2013). Finally, these data are averaged into 2° × 2° gridded boxes. We used the data set to assess the simulated cloud coverages and SLF. The analysis period is from June 2006 to March 2018.

2.2. MIROC6

2.2.1. General Model Description

We used two versions of the MIROC6 GCM: one is the version that participated in the CMIP6 (Tatebe et al., 2019), and the other is the latest version including a new precipitation parameterization (Michibata, Suzuki,

Sekiguchi, et al., 2019) described in Section 2.2.2. MIROC6 is coupled to the global aerosol module, Spectral Radiation-Transport Model for Aerosol Species (SPRINTARS; Takemura et al., 2000, 2002, 2005, 2009). SPRINTARS simulates mass mixing ratios of major tropospheric aerosol species, including black carbon, organic matter, sulfate, soil dust, sea salt, and precursor gases of sulfate.

MIROC6-SPRINTARS uses the probability density function (PDF)-based large-scale condensation (LSC) scheme, which considers the subgrid-scale fluctuations in temperature and total water content (Watanabe et al., 2009). The LSC scheme is combined with the ice micro-physical scheme proposed by Wilson and Ballard (1999), which treats cloud ice as a prognostic variable. The model uses a two-moment bulk scheme that involves both the mass and number mixing ratios of liquid droplets and ice crystals (Takemura et al., 2009).

2.2.2. Diagnostic and Prognostic Precipitation

Many GCMs, including MIROC, treat precipitation diagnostically, which assumes that it reaches the surface instantaneously and does not remain in the atmosphere in the next time step in the model calculation (Ghan & Easter, 1992). If the models explicitly simulate the fall velocity of the precipitation v, the Courant-Friedrichs-Lewy (CFL) criterion, which is defined as $v\Delta t/\Delta z < 1$, must be satisfied for numerical stability (Δt is the model timestep and Δz is the vertical model resolution). The DIAG scheme helps to avoid the restriction of the CFL criterion in the sedimentation process of precipitating hydrometeors. However, the DIAG scheme is unsuitable for drizzle and snow, which do not actually reach the surface within one model time step (10–20 min in general). This overemphasizes the auto-conversion process and underestimates the accretion process. The former depends on aerosol concentrations whereas the latter does not (Posselt & Lohmann, 2008), resulting in overly strong aerosol-cloud interactions in the DIAG scheme models (Gettelman et al., 2013; Jing et al., 2019).

To solve this problem, the PROG scheme, called CHIMERRA (Cloud/Hydrometeors Interactive Module with Explicit Rain and Radiation), was introduced into the latest version of MIROC6 (Michibata, Suzuki, Sekiguchi, et al., 2019). The two-moment PROG scheme prognoses rain and snow for their mass and numerical mixing ratios. The auto-conversion and accretion schemes are based on Khairoutdinov and Kogan (2000). The radiative effect for rain and snow is also considered by CHIMERRA.

2.3. Satellite Simulator (COSP2) and Precipitation Phase Diagnosis

The direct comparison between native model outputs and satellite retrievals causes uncertainties, due to the mismatch in scale between the model and observations, as well as retrieval assumptions (Bodas-Salcedo et al., 2011). For a consistent comparison between the model and satellite observations, COSP software was used in this study.

COSP divides the GCM grid mean profile into sub-columns with the Subgrid Cloud Overlap Profile Sampler (Klein & Jakob, 1999). In this study, we generated 140 sub-columns in the model to mimic the satellite pixel scales. Instrument simulators replicate synthetic retrievals of individual observations using ISCCP (Klein & Jakob, 1999; Webb et al., 2001), MISR (Marchand & Ackerman, 2010), PARASOL (Konsta et al., 2016), MODIS (Pincus et al., 2012), CALIPSO (Chepfer et al., 2008), and CloudSat (Haynes et al., 2007) simulators. COSP summarizes statistics based on individual simulators into output histograms and diagnostics (e.g., Michibata, Suzuki, Ogura, & Jing, 2019).

A key diagnostic to comprehensively evaluate cloud and precipitation is available from the CloudSat CPR and corresponding simulator (Quickbeam; Haynes et al., 2007). To diagnose the near-surface precipitation frequency and hydrometeor species, Kay et al. (2018) introduced a precipitation flag into COSP2 that is consistent with the CloudSat 2C-PRECIP-COLUMN product. Table 2 provides a definition of the precipitation flag in COSP2. The integer flag values are categorized based on the ice fraction, surface air temperature, and radar reflectivity, with thresholds that differ with the surface types (i.e., land [Haynes et al., 2009] or ocean [Smalley et al., 2014]). The definition follows the CloudSat precipitation flag retrievals in 2C-PRECIP-COLUMN, which enables a consistent comparison of precipitation frequency between CloudSat retrievals and climate model outputs, which ensures the evaluation is "scale aware" and "definition aware." This is consistent with our objective of assessing the Arctic precipitation system, where liquid-, solid-, and mixed-precipitation are frequently observed (McIlhattan et al., 2020, 2017).

Table 3
Details of the Tuning Experiment ("l", "i", "s", and "v" Are the Cloud Liquid, Cloud Ice, Snow, and Vapor, Respectively)

Tuning parameter	Factor	Relevant process	Meaning
(1) *bfice*	×0.1	BF process ($l \rightarrow i$)	Factor for water vapor diffusion coefficients
(2) *bfsnow*	×0.1	BF process ($l \rightarrow s$)	Factor for water vapor diffusion coefficients
(3) *csiaut*	×2	Auto-conversion ($i \rightarrow s$)	The particle size threshold between cloud ice and snow
(4) *eauti*	×0.1	Auto-conversion ($i \rightarrow s$)	Factor for changing rate of mass mixing ratio
(5) *tsauti*	×2	Auto-conversion ($i \rightarrow s$)	Timescale for crystal-to-snow conversion
(6) *depsubi*	×0.1	Deposition and sublimation ($v \leftrightarrow i$)	Factor for changing rate of mass mixing ratio
(7) *dnfsubi*	×10	Sublimation ($i \rightarrow v$)	Factor for changing rate of number mixing ratio
(8) *subs*	×10	Sublimation ($s \rightarrow v$)	Factor for changing rate of mass mixing ratio
(9) *vfcts*	×0.5	Snowfall velocity	Factor for bulk fall velocity weighted by mass and number
(10) *vfcts*	×1.5	Snowfall velocity	Factor for bulk fall velocity weighted by mass and number

2.4. Experimental Design

Simulations using the DIAG and PROG schemes were performed with prescribed sea surface temperatures and sea ice extent under present-day conditions. The COSP simulator was turned on after a 5 yr spin-up, and run for 1 yr to examine the seasonal variations. The model resolution is T85 (approximately 1.4° in longitude and latitude), with 40 vertical levels. COSP2 was applied to the entire simulated region, including areas south of 82°S and north of 82°N where the A-Train does not pass. We, therefore, define the Arctic region as 67°–82°N.

In the PROG scheme simulation, a suite of sensitivity experiments was carried out to examine how the uncertain tuning parameters link to the model-observation discrepancy. The model configuration other than the tuning parameters is the same as the control PROG scheme experiment (CTRL), and the details are summarized in Table 3. The (1) *bfice* and (2) *bfsnow* are scale factors of the water vapor diffusion coefficients in the Bergeron-Findeisen process (Bergeron, 1935; Findeisen, 1938) for the growth of cloud ice and snow, respectively. For the auto-conversion process that produces snow due to collisions of cloud ice, (3) *csiaut*, (4) *eauti*, and (5) *tsauti* are the particle size threshold between cloud ice and snow, a scale factor, and the timescale for crystal-to-snow conversion, respectively. For the processes that occur between cloud ice and vapor, (6) *depsubi* relates to the deposition of vapor or sublimation of cloud ice, and (7) *dnfsubi* is the parameter for changing the values of the number mixing ratios. Sublimation of snow is controlled by (8) *subs*. The parameter (9), (10) *vfcts* is a scale factor for the terminal snowfall velocity. The results are presented in Section 3.5.

We also performed nudged simulations for 2007–2008, where horizontal winds and temperatures were nudged toward ERA-Interim reanalysis data to identify whether the model bias is from the environmental or physics schemes. The 2008 data were used for the subsequent nudged model analysis and compared with the observations, as discussed in Section 3.3 (Figure S2 in Supporting Information S1).

3. Results

3.1. Warm Clouds

As reported in recent studies, the modeling approach of the PROG scheme improves the cloud-to-rain conversion (Michibata & Suzuki, 2020) and the magnitude of aerosol-cloud interactions (Gettelman et al., 2015; Michibata et al., 2020), which are in better agreement with satellite observations. These evaluations have mainly been conducted for low- and mid-latitude warm clouds, to understand their link to aerosols. However, little is known about the impact of different precipitation parameterizations on high-latitude cloud biases. Here, we examined the difference in warm cloud representation between the DIAG and PROG schemes over the Arctic, where the hydrometeor phase is susceptible to the thermodynamic conditions (Morrison et al., 2012; Zamora et al., 2018). For simplicity, we extracted the single-layer warm clouds (SLWCs) from the COSP output and satellite retrievals following Michibata, Suzuki, Ogura, et al. (2019). Following Michibata et al. (2016), the cloud layer was defined as being where the CPR cloud mask is >30, CPR radar reflectivity is higher than −30 dBZe, MODIS cloud

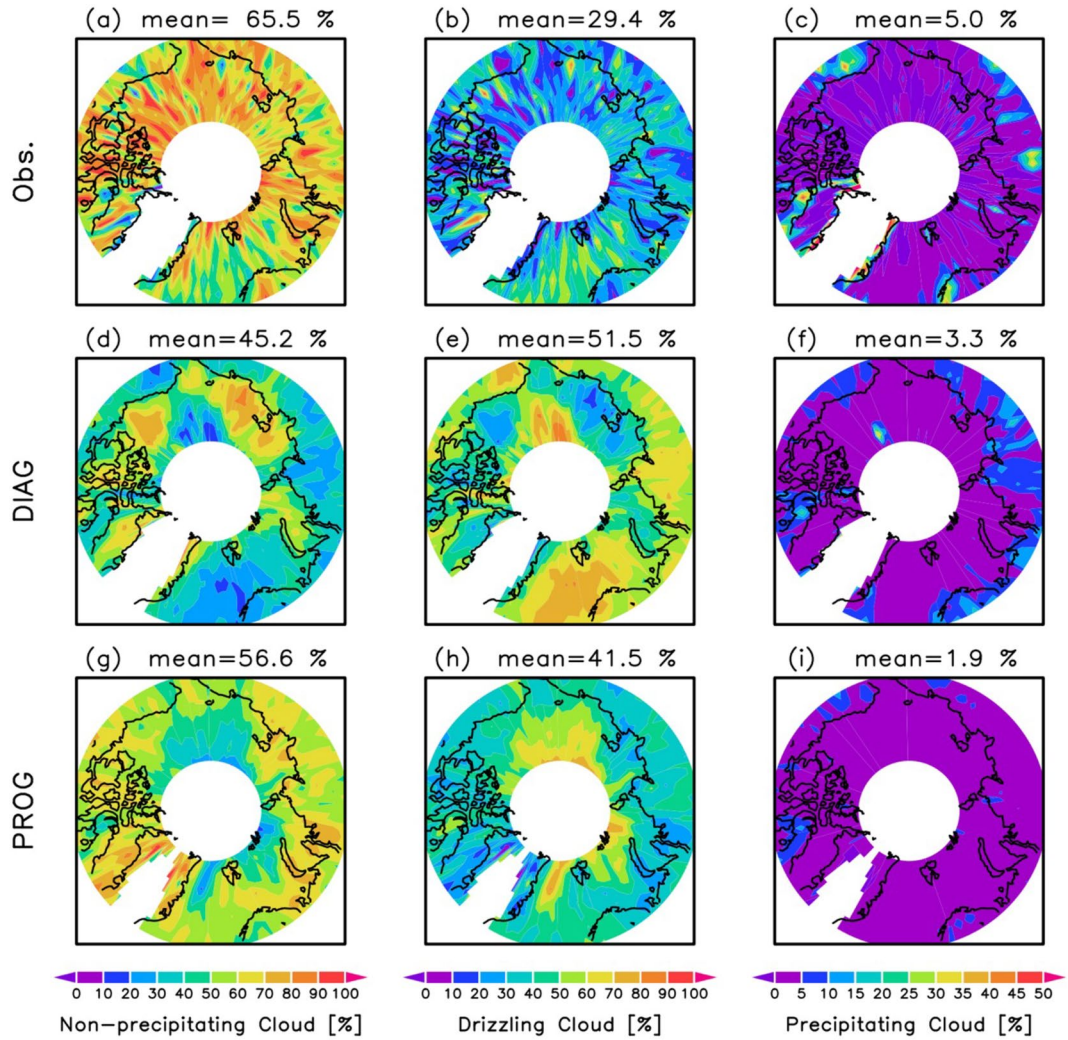

Figure 1. Annual averages of the relative occurrence frequency of (a, d, g) non-precipitating clouds, (b, e, h) drizzling clouds, and (c, f, i) precipitating clouds for Arctic warm clouds obtained from (a–c) A-Train observations, and the (d–f) MIROC6 DIAG and (g–i) MIROC6 PROG scheme simulations. Area-weighted averages over the Arctic are shown above each panel. Note that the region north of 82°N is masked for the model simulations to match the observational area.

optical depth is >0.1 (within an uncertainty of <5), and the MODIS cloud effective radius is 5–35 μm (within an uncertainty of <1 μm). We used SLWCs with cloud top temperatures of >273.15 K.

Figure 1 shows the occurrence frequencies of the non-precipitating, drizzling, and precipitating clouds obtained from the A-Train observations, DIAG scheme, and PROG scheme over the Arctic. These three types of cloud regime are classified by the CloudSat column maximum radar reflectivity (Z_{max}) as follows: $Z_{max} < -15$ dBZ$_e$ for non-precipitating clouds; -15 dBZ$_e$ $< Z_{max} < 0$ dBZ$_e$ for drizzling clouds; and $Z_{max} > 0$ dBZ$_e$ for precipitating clouds. SLWCs are rare in the Arctic (annual average of 1.7% of all Arctic single-layer clouds), but the SLWCs in this region are important because of (a) the high magnitude of aerosol-cloud interactions (Coopman et al., 2018) and (b) regime-dependent LWP adjustment (Murray-Watson & Gryspeerdt, 2022).

Although significant underestimation of the frequency of the non-precipitating regime was found with both the DIAG and PROG schemes as compared with the A-Train observations (65.5%), the DIAG scheme (45.2%) performed more poorly than the PROG scheme (56.6%; Figures 1a, 1d, and 1g). The PROG scheme performs well in simulating the frequency over continental regions and the Greenland Sea, which DIAG underestimates, whereas over the East Siberian Sea and periphery of 82°N the occurrence frequency is less than the observation. For the drizzling regime, the annual averages of the occurrence frequency are over-represented in both versions of

MIROC, indicating that the "too frequent and too light" warm rain bias (Stephens et al., 2010; Suzuki et al., 2015) still exists over the Arctic region. However, the PROG scheme simulation (41.5%) is more similar to the A-Train observations (29.4%) than the DIAG scheme simulation (51.5%), especially for continental regions and the Greenland Sea (Figures 1b, 1e, and 1h), along with the non-precipitating regime. Although some biases also exist in the precipitating regime (Figures 1c, 1f, and 1i), this regime seldom dominates, and thus is less important over the Arctic. Therefore, the fact that the PROG scheme yields occurrence frequencies of the non-precipitating and drizzling regimes (which dominate the Arctic) that are in better agreement with the A-Train observations suggests this scheme provides an improved representation of Arctic warm clouds.

3.2. Cloud Coverage and Snowfall

Figure 2 shows the spatial distributions of annual mean cloud coverage for total-, high-, middle-, and low-level clouds from CALIPSO-GOCCP observations, and the DIAG and PROG scheme simulations. Total cloud coverage is significantly underestimated by the DIAG scheme relative to the observations (Figures 2a and 2b), reflecting a "too few" cloud bias that is a common problem for the tropics in GCMs (Nam et al., 2012), and is also the case over the Arctic in the traditional MIROC DIAG scheme. This result is consistent with previous studies (e.g., English et al., 2015; Kay et al., 2012; McIlhattan et al., 2020). However, the PROG scheme simulation reproduces the observed cloud cover, particularly over the Barents Sea and continental regions, as well as averages over the Arctic region (Figure 2c). For the high-level cloud, the DIAG scheme underestimates for all the Arctic regions, while the geographical distribution from the PROG scheme, especially in continental regions, is consistent with the observations (Figures 2d–2f). Similarly, middle-level cloud over most of the Arctic regions is underestimated with the DIAG scheme (14.8%), but is more than doubled in the PROG scheme (34.3%) and closer to observations (27.7%; Figures 2g–2i). Finally, the distribution and averages of the low-level cloud from the PROG scheme are similar to observations (Figures 2j–2l).

Figure 3 shows the monthly mean cloudiness from the CALIPSO-GOCCP observations and two versions of MIROC, along with the root mean squared error (RMSE) with respect to the observation. Focusing on the total cloud coverage, the underestimation is up to 20% smaller than the observations from the DIAG scheme, whereas the PROG scheme performs better during all months (Figure 3a). The annual cycle of high-level cloud coverage, which increases in summer and decreases in winter, is also well reproduced by the PROG scheme, but is not evident in the DIAG scheme simulation (Figure 3b). Although the middle-level cloud coverage is slightly overestimated by the PROG scheme simulation, the annual cycle is much closer to the observed trend as compared with the DIAG scheme simulation (Figure 3c). For the low-level cloud coverage (Figure 3d), the PROG scheme simulation produces more realistic values than the DIAG scheme simulation, and is almost the same as the observations from January to March. Low-level cloud coverage varies widely according to the season and has a large effect on the total cloud coverage and its seasonal changes. The RMSEs for the PROG scheme are smaller than those for the DIAG scheme, which indicates the former performs better in modeling in the Arctic cloudiness.

Figure 4 shows maps of annual mean snowfall rates in the Arctic, as obtained from the CloudSat observations, and DIAG and PROG scheme simulations. The annual average snowfall rate from the PROG scheme simulation (249.1 mm yr^{-1}) is closer to the observation (254.5 mm yr^{-1}) than is the DIAG scheme simulation (230.9 mm yr^{-1}). This is consistent with the improvement of cloud coverage as shown in Figures 2 and 3. In terms of the geographic distributions, although the DIAG scheme simulation accurately reproduces the snowfall rates in Siberia and Canada, it underestimates the rates in the periphery of Greenland, where the PROG simulation shows a better performance.

The monthly mean snowfall rates and observational uncertainty, which are available from the CloudSat 2C-SNOW-PROFILE (Wood et al., 2014), are shown in Figure 5. Both the DIAG and PROG scheme simulations adequately reproduce the observed seasonal cycle (i.e., low snowfall in summer and high snowfall in winter) and are generally within the observational range, but they both have a positive bias in summer and negative bias in winter. These biases are smaller for the PROG scheme simulation, given it has smaller RMSEs than does for the DIAG scheme, suggesting that the model performance for snowfall rates is improved by using the PROG scheme, with regards to both annual and monthly averages. This is likely linked to the improved cloudiness in the PROG scheme (Figure 3).

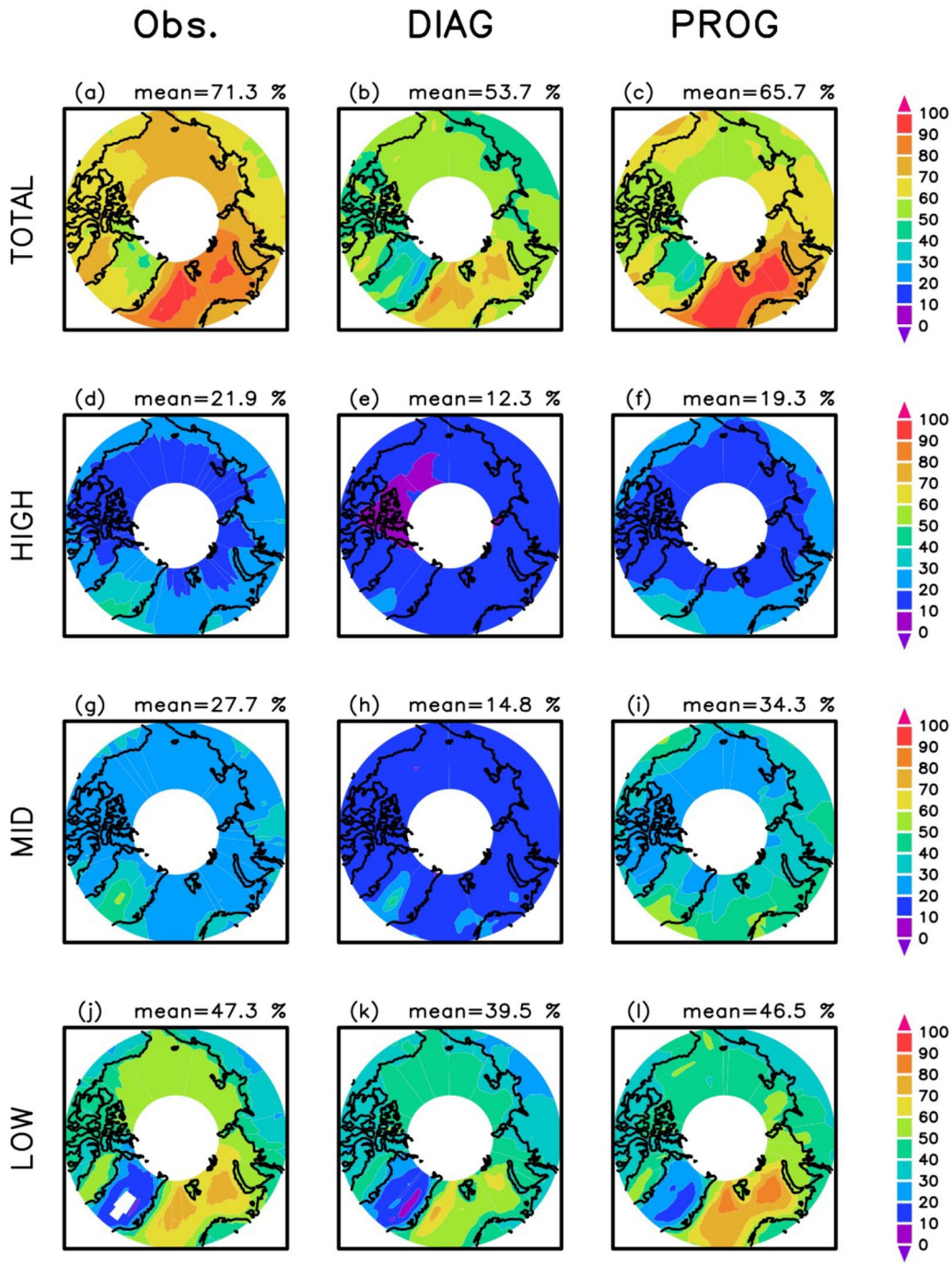

Figure 2. Annual mean geographic distributions of (a–c) total, (d–f) high-level, (g–i) middle-level, and (j–l) low-level cloud coverage over the Arctic obtained from (a, d, g, j) CALIPSO-GOCCP observations, and (b, e, h, k) MIROC6 DIAG and (c, f, i, l) MIROC6 PROG scheme simulations. The averages over the Arctic region are shown above each panel. The area north of 82°N is masked for the model simulations to match the observational area.

3.3. Precipitation Frequency and Phase Partitioning

Although we obtained improved representations of Arctic warm clouds, cloud coverage, and snowfall rate with the PROG scheme, it is unclear how frequently and what types of hydrometeors fall to the surface. To understand their effects on Arctic climate, we assessed the morphology of near-surface precipitation following Kay et al. (2018), who introduced a new diagnostic method using a precipitation flag. The precipitation flag provides

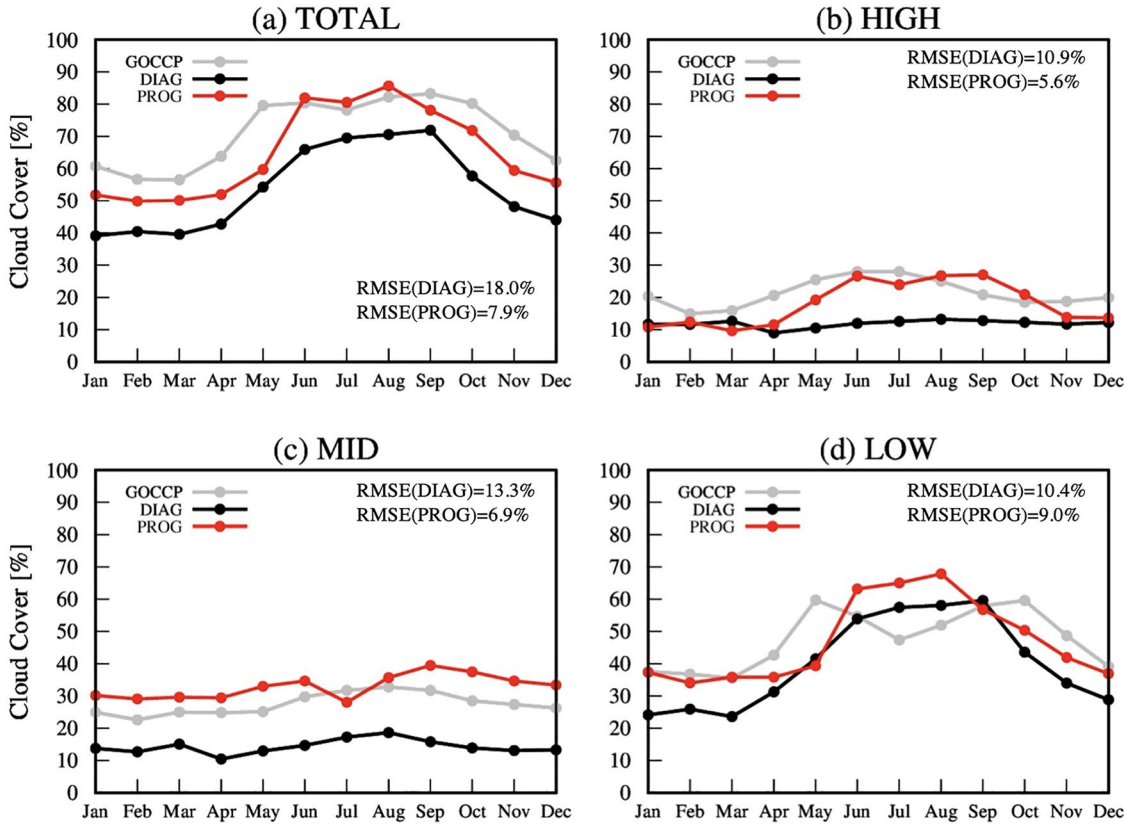

Figure 3. Annual cycle of (a) total, (b) high-level, (c) middle-level, and (d) low-level cloud cover over the Arctic. The gray, black, and red lines correspond to CALIPSO-GOCCP observations, and DIAG and PROG scheme simulations, respectively. Root mean squared errors (RMSEs) were calculated from the average differences in the monthly mean cloud cover between the models and observations.

information on the precipitation type and intensity, and is now available in MIROC6 via the COSP2 simulator (Table 2). The occurrence frequency of each precipitation phase i ($\in$ flag 0–9; Table 2) at longitude (λ) and latitude (ϕ) is defined as follows:

$$f_i(\lambda,\phi) = \frac{n_i(\lambda,\phi)}{n(\lambda,\phi)}, \tag{3}$$

where n is the total number of samples.

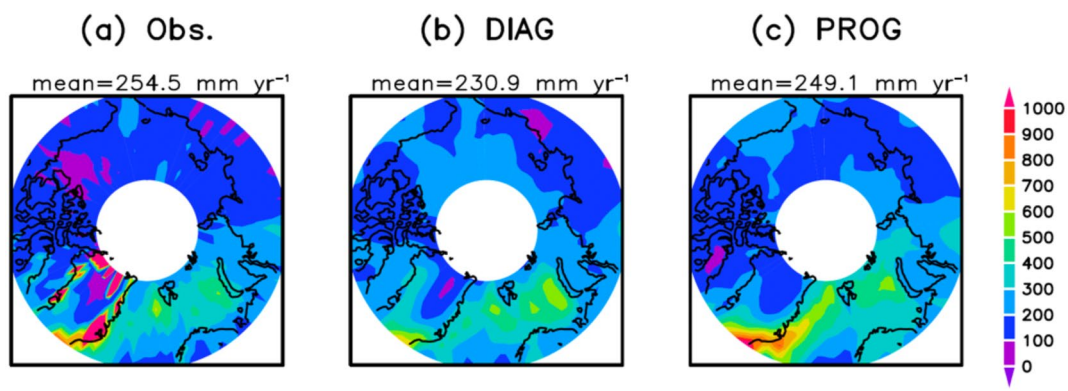

Figure 4. Geographic distributions of snowfall rate (mm yr^{-1}) obtained from (a) CloudSat 2C-SNOW-PROFILE, and the (b) DIAG and (c) PROG scheme simulations. The Arctic averages are shown above each panel. The area north of 82°N is masked for the model simulations to match the observational area.

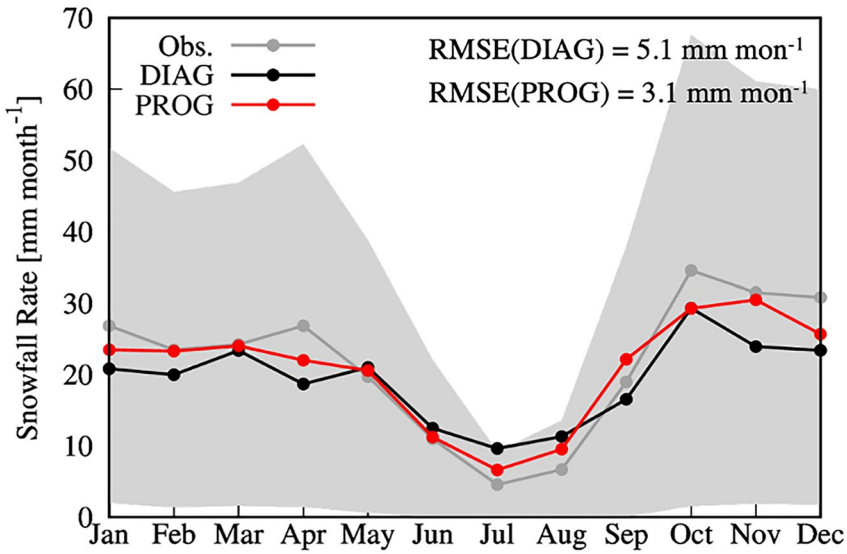

Figure 5. Annual cycle of the snowfall rate (mm month^{-1}) in the Arctic obtained from (a) CloudSat 2C-SNOW-PROFILE, and the (b) DIAG and (c) PROG scheme simulations. The CloudSat observations, and DIAG and PROG simulations are shown as gray, black, and red lines, respectively. Root mean squared errors (RMSEs; top right) were calculated from the monthly mean snowfall rate as compared with the observations, and the gray shading indicates the observational uncertainty.

Figure 6 shows the geographic distributions of the annual mean occurrence frequencies of each precipitation phase. We define the frequencies of no precipitation, rain, light snow, snow, and mixed precipitation as flags 0, 3, 4, 5, and 7, respectively. It should be noted that the diagnosis includes clear sky scenarios.

The non-precipitation frequency is better reproduced by the DIAG scheme simulation (Figures 6a–6c). Figure 6 obtained from the precipitation flags includes both clear and cloudy scenes, whereas Figure 1 only considered SLWCs without clear sky conditions, which accounts for the apparent inconsistency between these two figures. The frequency of non-precipitating clouds is underestimated by >20% in the PROG scheme simulation, in which snowing clouds are frequently observed in the Arctic (Figures 6d–6i). In detail, the PROG scheme simulation overestimates the occurrence frequency of light snow (12.9%) as compared with the DIAG scheme simulation (8.5%) and observations (8.9%; Figures 6d–6f). However, the bias with the PROG scheme is larger for the snow category, particularly for Greenland and the Barents Sea (Figures 6g–6i). The bias is mainly due to the snow intensity and/or snowflake diameter, which is discussed later. For the rain and mixed precipitation, the occurrence frequencies for the models and observations are much lower than the snow phases. Both the DIAG and PROG schemes accurately reproduce the observational averages (Figures 6j–6o). Figure S2 in Supporting Information S1 is the same as Figure 6, but for the observations and nudged simulations for 2008. The occurrence frequencies of snow categories from the PROG scheme still disagree with that for the observations, implying that the principal source of the snow biases is the modeled microphysical processes rather than environmental components.

To understand the model bias in Arctic precipitation occurrence frequencies, we examined the seasonal cycle (Figure 7). The precipitation types were classified into five categories: (a) no precipitation (flag 0); (b) rain (flags 1–3 and 8); (c) snow (flags 4 and 5); (d) mixed precipitation (flags 6 and 7); and (e) uncertain precipitation (flag 9). These precipitation types ignore the precipitation intensity. The observations show that the snow occurrence frequency is higher from winter to spring and lower from summer to autumn, when it is replaced by rain and mixed precipitation, which is consistent with the seasonal pattern of precipitation rate (Figure 5). This feature is also evident from the models, but the ratios of rain, snow, and mixed precipitation from the PROG scheme simulation show marked seasonal changes. This implies that surface precipitation from the PROG scheme simulation is more susceptible to the surrounding environment (e.g., temperature) due to melting, riming, and collection processes. In addition, snow from the PROG scheme simulation is overly frequent in any season. This indicates that the PROG scheme simulation produces more frequent snow than the observations and the DIAG scheme simulation. The reason for this is discussed in Section 3.5.

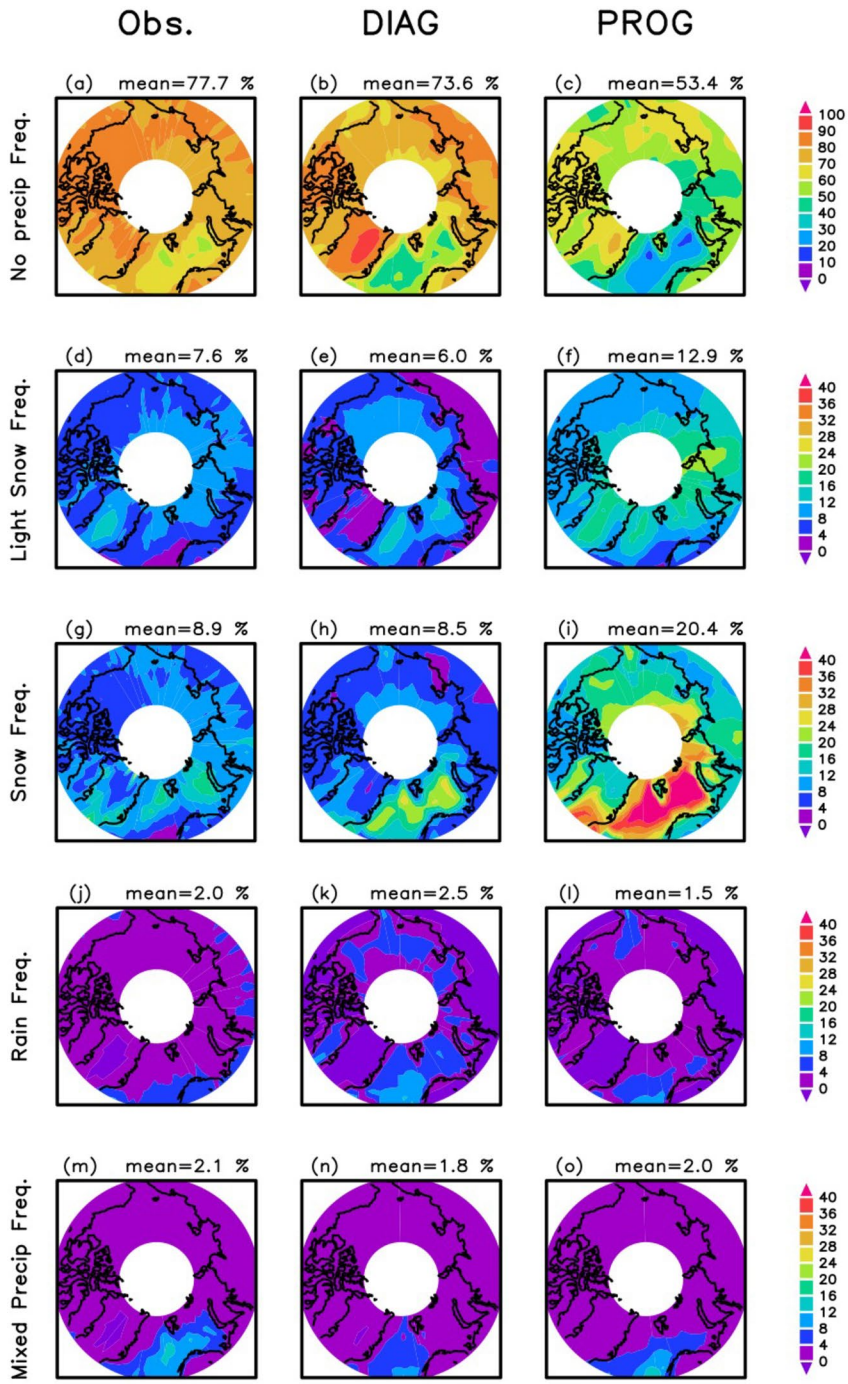

Figure 6. Annual mean near-surface frequencies of (a–c) no precipitation (flag 0), (d–f) light snow (flag 4), (g–i) snow (flag 5), (j–l) rain (flag 3), and (m–o) mixed precipitation (flag 7) in the Arctic, obtained from (left) CloudSat observations, and (center) DIAG and (right) PROG scheme simulations. The area north of 82°N is masked for the model simulations to match the observational area.

3.4. Seasonal Biases in Precipitation Intensity

As described in the previous sections, the PROG scheme simulation has biases in the near-surface precipitation frequency and its partitioning, even though the cloudiness and surface snowfall rates are in better agreement with the observations. These results suggest that the correct cloud coverage and snowfall rates can be achieved by compensating the errors with the precipitation frequency and intensity in the model, which will introduce further

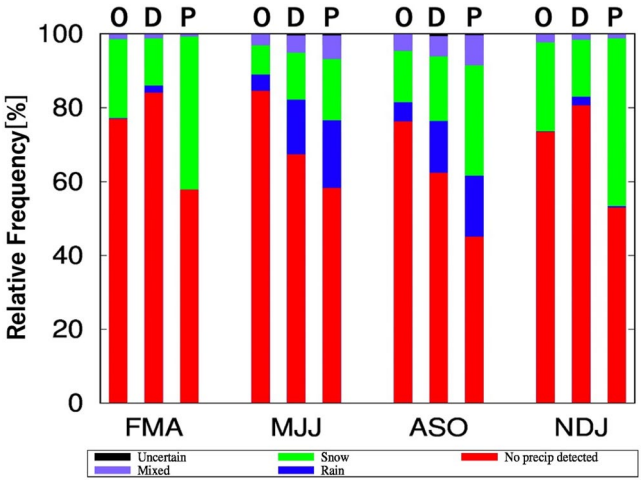

Figure 7. Seasonal averages of near-surface precipitation frequencies for no precipitation (red), rain (blue), snow (green), mixed precipitation (purple), and uncertain precipitation (black) in the Arctic, obtained from observations (O), and the DIAG (D) and PROG (P) scheme simulations. Seasons are as follows: spring (FMA; February–April), summer (MJJ; May–July), autumn (ASO; August–October), and winter (NDJ; November–January).

uncertainties into the climate simulation. To understand the reason for the biases in snowfall occurrence in the context of the hydrological cycle, we must understand how cloud ice contributes to consequent snowfall. As such, we attempted to link the IWP and snowfall rates simultaneously to examine the source of the discrepancy in the precipitation efficiency between the model and observations. The CloudSat IWP was used for the observations, whereas the MODIS IWP was used for the model analysis, since the CloudSat IWP is not available in the current Quickbeam. Although the CloudSat IWP is generally higher than the MODIS IWP, the difference is relatively small over the Arctic region (Eliasson et al., 2011), and this uncertainty is not discussed in this paper. This inconsistency should be avoided in future studies.

The link between the IWP and snowfall intensity was examined from the joint PDF of the IWP and snowfall rate (Figure 8). Although the observed distributions of high-frequency areas in summer and autumn show a slight shift toward the top right as compared with those in spring and winter, the PDFs are largely seasonally independent (Figures 8a, 8d, 8g, and 8j). This implies that snowfall over the Arctic is primarily controlled by the IWP. The DIAG and PROG scheme simulations capture the observed characteristics, but the models tend to simulate a lower snowfall rate. This is evident in the PROG scheme simulation, which rarely generates strong snowfall, even in the case

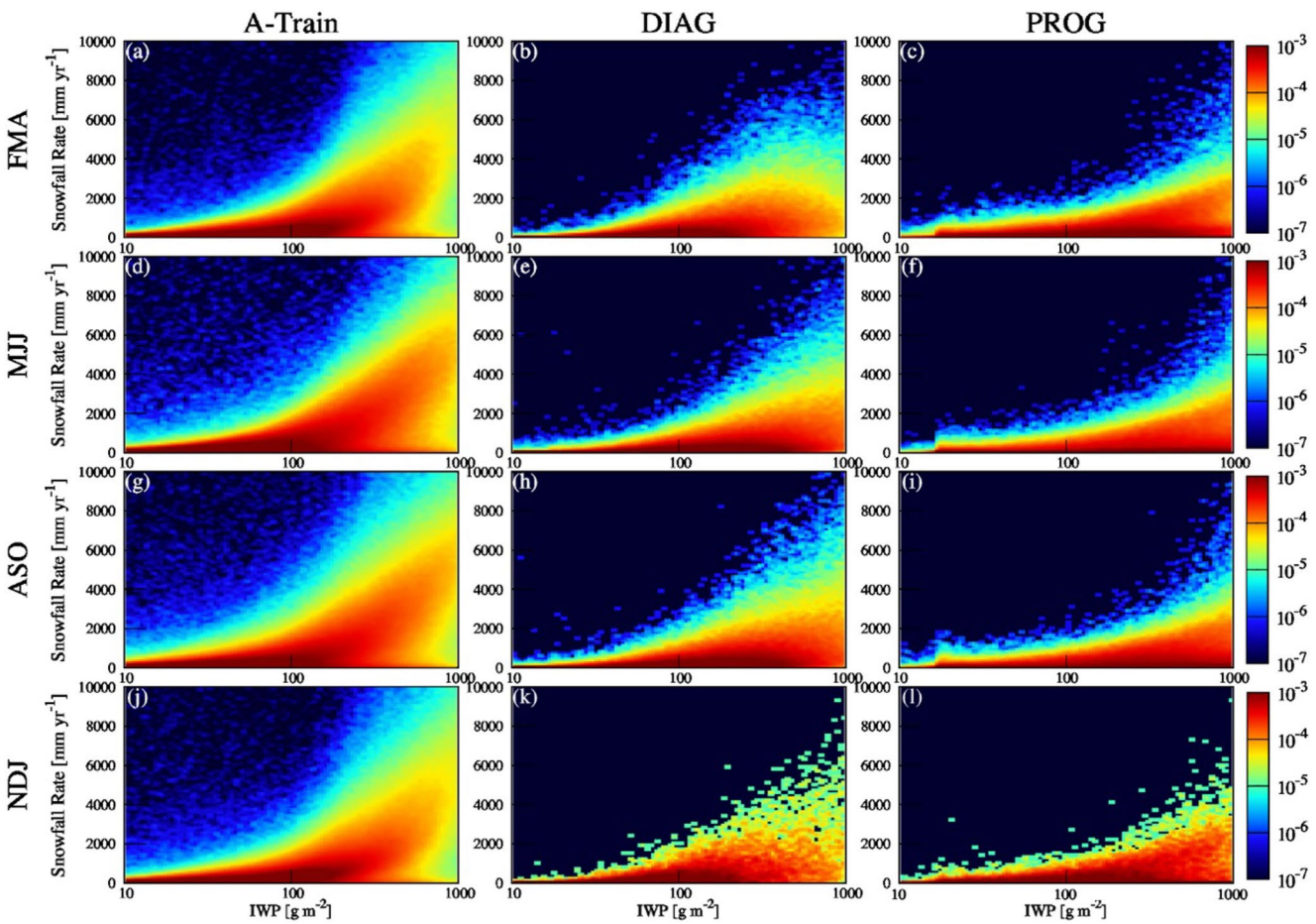

Figure 8. Seasonal variations in the probability density function (PDF) of the ice water path (IWP) and snowfall rate in the Arctic obtained from (a, d, g, j) A-Train observations, and (b, e, h, k) DIAG and (c, f, i, l) PROG scheme simulations. Note that the *x*-axis for the IWP and colored shading have logarithmic scales.

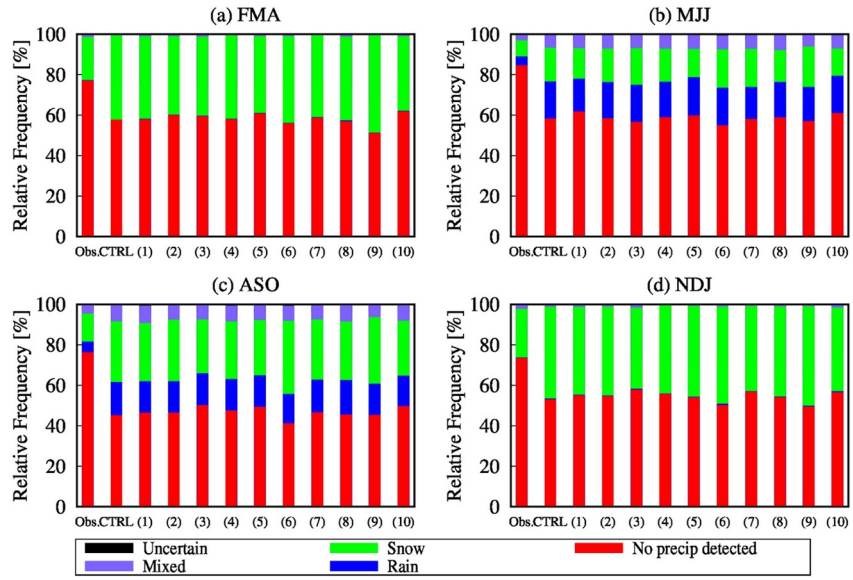

Figure 9. Relative frequency of precipitation phase partitioning for (a) FMA, (b) MJJ, (c) ASO, and (d) NDJ from observations (Obs.) and MIROC PROG simulations of the CTRL experiment and a suite of sensitivity experiments. The numbers in parentheses correspond to the configuration described in Table 3. The seasonal mean frequencies of no precipitation (red), rain (blue), snow (green), mixed precipitation (purple), and uncertain precipitation (black) in the Arctic are shown.

when the IWP exceeds 100 g m^{-2} (Figures 8c, 8f, 8i, and 8l), and is consistent with the "too frequent and too light" snowfall bias of the PROG scheme simulation (Figure 6). These results suggest compensating errors exist in the PROG scheme simulation, which yield a realistic annual mean cloud coverage and snowfall rate, despite the "too frequent and too light" snowfall bias over the Arctic. This is similar to the well-known bias in the tropics.

3.5. Links Between Model Biases and Tuning Parameters

To understand the source of the compensating errors described above, we conducted a suite of sensitivity experiments by perturbing the tuning parameters for the processes involving snow and cloud ice. In these experiments, values for the tuning parameters, which are the semi-empirical and physical parameters attributed to various assumptions in the parameterization of GCMs, were changed within the range of their uncertainties as summarized in Table 3. The parameters (1) *bfice* and (2) *bfsnow* for the BF process were reduced by a factor of 0.1 following Lawson and Gettelman (2014), to achieve a better agreement with observations. The parameter (3) *csiaut* controls the initiation of the ice-to-snow conversion, with a larger *csiaut* allowing more cloud ice and less snow (Eidhammer et al., 2014); it also controls the ice-to-snow auto-conversion timescale. The parameter (5) *tasuti*, behaves in a similar fashion (Morrison & Gettelman, 2008), whereas parameter (4) *eauti* is a simple unphysical factor utilized in the conversion efficiency. Although the parameters for deposition and sublimation, which are (6) *depsubi*, (7) *dnfsubi*, and (8) *subs*, should not be tuned because these processes are thermodynamically determined, we also examined these sensitivities for comparison with other micro-physical processes. The varied values for (9), (10) *vfcts* were determined such that the snowfall velocity was higher than that of cloud ice and lower than that of raindrops. The results are detailed in Table S1 in Supporting Information S1.

Figure 9 shows the occurrence frequencies of each precipitation type (i.e., no precipitation, rain, snow, mixed precipitation, and uncertain) as in Figure 7. In comparison with the CTRL, the snow frequency has a relatively high sensitivity to the parameters (9) and (10) *vfcts* in all seasons, which implies that snow formation in the PROG scheme simulation is susceptible to snowfall velocity. For each season, (5) *tsaut* shows a slight improvement in spring and summer as a result of limits to snow formation by crystal-to-snow auto-conversion. We also found somewhat better results for (3) *csiaut* in autumn and winter, as only larger crystals contribute to producing snow. Nevertheless, the dramatic changes necessary to make the frequencies for the CTRL simulation equivalent to the observational frequencies were not obtained. This implies that there are fundamental uncer-

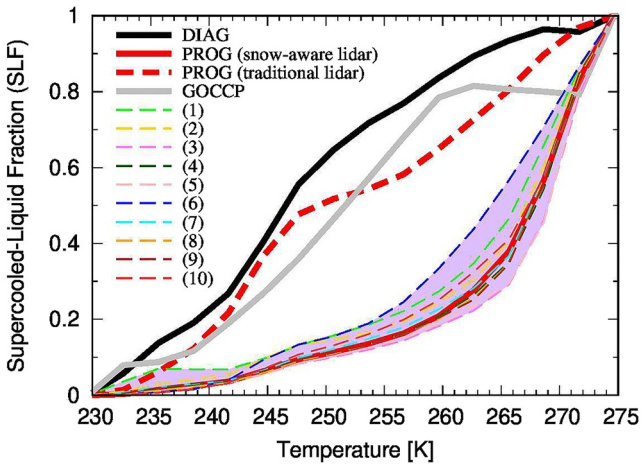

Figure 10. Supercooled liquid fraction (SLF) as a function of temperature in Arctic clouds for the CALISPO-GOCCP observations (solid gray line), and DIAG (solid black line) and PROG (colored lines) scheme simulations. The solid and dashed red lines indicate the snow-aware and traditional LiDAR simulations in the PROG scheme, which account for and ignore snowflakes near clouds in the SLF diagnostic, respectively. The other dashed lines represent the tuning experiments in the snow-aware PROG scheme simulation.

tainties in the cloud and precipitation representations, such as the dynamics, thermodynamics, and turbulence (e.g., Eirund et al., 2019; Feist et al., 2019; Korolev & Field, 2008; Shupe et al., 2013), as well as the sub-grid-scale ice representation.

In addition to evaluation of precipitation phase partitioning, it is essential to examine the cloud phase partitioning, which has a significant role in Arctic climate (Avramov & Harrington, 2010; Cesana et al., 2021; Morrison et al., 2009; Zhang et al., 2019). Figure 10 shows the dependence of SLF on temperature in Arctic mixed-phase clouds. The SLF decreases with decreasing temperature, but the rate of decrease is quite different between the DIAG and PROG scheme simulations, and also between the snow-aware and traditional LiDAR simulations in the PROG scheme. The DIAG and traditional PROG scheme simulations that are not snow-aware produce the observed trend, whereas the snow-aware PROG scheme simulations have a much lower SLF than the observations. Given that the SLF increases significantly by switching from the snow-aware to traditional LiDAR simulations for the CTRL experiment (Figure 10), all the tuning experiments yield results more consistent with the observations (not shown), depending on how much cloud ice is included in the model.

In one tuning experiment, (1) *bfice* shows a slight improvement because cloud ice formation by the BF process is constrained by changing the value to one tenth of the default value. We observed the strongest sensitivities for (6) *depsubi*, which affects the balance of sublimation of cloud ice and vapor deposition. Other experiments also show a slight improvement (e.g., (2) *bfsnow*, (10) *vfcts*); however, all the SLF results from the model tuning remained much lower than the observations. These results show that the PROG scheme simulation results in a significant underestimate of the SLF and overestimates the ratios of cloud ice. Given that the PROG precipitation effectively increases the Arctic cloudiness as compared with the DIAG precipitation (Figures 2 and 3), the lower SLF is possibly linked to the overestimation of snow frequency. Although some GCMs include PROG precipitation, the frequent snowfall generated by our MIROC model also appears to characterize some other models (e.g., the CESM model; McIlhattan et al., 2020).

Figure 11 is a schematic diagram that explains the difference between the two model schemes. The SLF diagnostic in the DIAG scheme and PROG scheme with the traditional LiDAR simulations uses the ratio of cloud liquid water to total cloud water (i.e., liquid and ice; Figure 11a). Although this assumption appears not to be problematic, the latest version of the CALIPSO LiDAR simulator used in this study includes some snowflakes adjacent to clouds in the cloud phase diagnosis (Cesana et al., 2021). This is consistent with the actual LiDAR observations, because LiDAR retrieval cannot distinguish accurately between ice crystals and snowflakes. Therefore, unlike the DIAG scheme, snowflakes in the atmosphere are partly detected as a cloud layer by the PROG scheme (Figure 11b). As a result, the PROG scheme has a high total water content that is the denominator for the calculation of the SLF, which leads to an apparent deterioration of the cloud phase diagnostics.

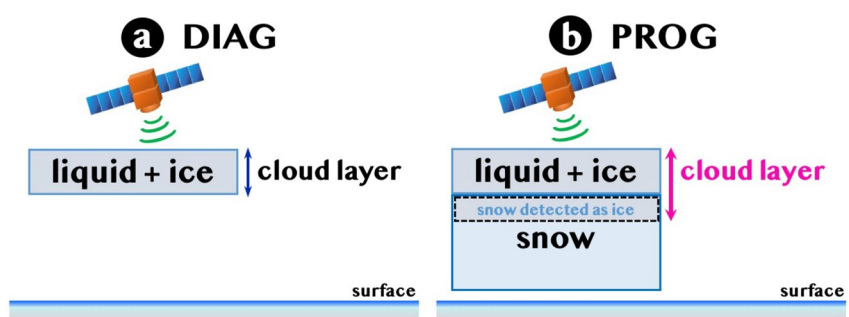

Figure 11. Schematic illustration of the difference in retrieval algorithm between the (a) DIAG and (b) PROG schemes for cloud detection with the LiDAR simulator.

4. Summary and Discussion

This study has examined phase partitioning of cloud and precipitation in the Arctic. To focus directly on the structural differences in the precipitation parameterization, we used two versions of the MIROC6 GCM: the conventional DIAG and updated PROG schemes. The model outputs were systematically compared with multi-satellite retrievals using the COSP2 satellite simulator.

The MIROC PROG simulation performed better by increasing the non-precipitating cloud and decreasing drizzling cloud occurrences for the Arctic warm cloud occurrences (Figure 1), increasing the cloud cover (Figures 2 and 3), and increasing the snowfall rates at the surface (Figures 4 and 5), as compared with the DIAG simulation. However, critical biases in Arctic precipitation and cloud phase partitioning still characterize the PROG simulation. Precipitation phase diagnostics using COSP2 (Kay et al., 2018; Swales et al., 2018) have revealed that the PROG scheme simulation produced a much higher frequency of annual mean Arctic snow, as observed in a previous study of the Greenland ice sheet (Lenaerts, Drew Camron, et al., 2020), implying faster snow formation. In addition, although the satellite-derived snowfall rates over the Arctic increased rapidly with increasing IWP, the MIROC GCM did not capture the strong snowfall, even for the larger IWP, particularly with the PROG scheme simulation (Figure 8). In addition to the annual biases outlined above, the ratios of snow, rain, and mixed-phase precipitation in the PROG scheme simulation are more sensitive to seasonal changes relative to the satellite observations (Figure 7), and exhibit a higher occurrence of rain in summer and snow in winter. These results suggest that the "too frequent and too light" Arctic snowfall bias appears due to switching the precipitation scheme from DIAG to PROG, which inadvertently produces realistic annual mean Arctic cloud cover and snowfall. The significant increase in the snow water path from the DIAG to PROG scheme (Figure S1 in Supporting Information S1) possibly results in the too frequent snowfall. This suggests that there are more fundamental errors in the conversion process from cloud ice to snow, which is an important area to explore in future model development (e.g., Milbrandt & Morrison, 2016).

The compensating errors identified in this study possibly exist in other GCMs, due to the simplified treatment of cloud and precipitation (Jing et al., 2019). If the models overestimate the occurrence frequency of snow, then the potential phase change from snow to rain will also be over-represented. The key point is that although snow has a large effect on the radiation budget through both the greenhouse and parasol effects (Li et al., 2019, 2020; Michibata, Suzuki, Sekiguchi, et al., 2019), the radiative effect of rain is negligible (Hill et al., 2018). Given the different radiative roles of rain and snow on in terms of climate, the precipitation phase change affects the climate sensitivity (Cesana et al., 2021). If snow is converted into rain that is less radiatively opaque as the climate warms, the incoming solar radiation at the surface and outgoing long-wave radiation will increase, driving a positive and negative feedback, respectively. This is one possible hypothesis based on a few limited models, but there is no consensus on the magnitude of these feedbacks and their mechanisms (Cesana et al., 2021; Hirota et al., 2022), due to uncertainties in our understanding and representation of aerosol-cloud-precipitation interactions (Michibata, 2022). However, the introduction of the PROG scheme increases the equilibrium climate sensitivity (ECS; e.g., Gettelman, Hannay, et al., 2019; Hirota et al., 2022).

One of the key causes of increased ECS is that the cloud altitude feedback is more evident in the PROG scheme due to the improved representations of the amount of cloud and its vertical structure, which result in the efficient longwave warming effect (Hirota et al., 2022). If we improve the bias in the precipitation phase partitioning by mitigating the too frequent snowfall by suppressing the ice-to-snow conversion, then the model enhances this positive cloud altitude feedback due to the increase in high-level cloud amount. However, the increased cloud ice can also induce a negative optical depth feedback (Tan et al., 2016). Although the net cloud feedback, including other processes, is highly model-dependent, multiple model results suggest that a positive cloud feedback will be dominant (e.g., Hirota et al., 2022; Wang et al., 2021; Zelinka et al., 2022, 2020).

However, the effects of the biases in the precipitation phase partitioning on the radiative feedback under warming remain controversial. A continuous study of how snowfall biases affect the radiative feedback would constrain the model uncertainties, such that more accurate climate predictions can be made. Given that the model biases were barely reduced by parameter tuning of the micro-physical processes (Figure 9), one cause of these discrepancies may be the surrounding environmental regimes (e.g., Gierens et al., 2020; Griesche et al., 2021), such as temperature, humidity, and wind. In this regard, it will be important to investigate the sensitivity of the biases to the vertical model resolution (Ingram & Bushell, 2021). Although we undertook nudged simulations, the results

suggested that environmental factors have less effect on the Arctic snowfall biases (Figure S2 in Supporting Information S1). Therefore, it is still necessary to improve the representation of micro-physical processes, because GCMs simply consider sub-grid-scale variability of cloud and precipitation and ignore larger precipitating hydrometeors (e.g., graupel), apart from some state-of-the-art models (e.g., MG3; Gettelman, Morrison, et al., 2019; Morrison et al., 2009).

In addition to the precipitation phase, this study also showed that the cloud phase diagnosis was strongly affected by changing the precipitation scheme. Our results indicate that the PROG scheme simulated lower SLF values for the Arctic than the CALIPSO observations and DIAG scheme. This is mainly attributable to increased total ice water due to prognosed snow, part of which is regarded as being cloud ice in the simulator (Cesana et al., 2021). The increased cloud ice, as well as cloud cover, in the PROG scheme can be a cause of the excess snowfall. To address this issue, a further study of the accurate mass ratios between snowflakes and cloud ice used in the cloud phase diagnostics should be undertaken. In addition, if satellite observations count in-cloud snow as part of the total water, then the satellites and models might yield erroneously consistent results when GCMs use a DIAG scheme. This means that the latent bias in the SLF exists in most of the CMIP6 models, although recent studies have reported improvements in SLF simulations (Mülmenstädt et al., 2021; Zelinka et al., 2020). In addition, GCMs that underestimate the SLF will underestimate climate sensitivity due to a stronger negative feedback mechanism (Tan et al., 2016). Thus, it is necessary to examine how the biases in both the cloud and precipitation phase partitioning are linked to climate feedback in a warming climate.

We have found that the more sophisticated PROG scheme simulation still has biases in precipitation and cloud phase partitioning, and their occurrence frequency, over the Arctic. There is a "too frequent and too light" snowfall bias with inaccurate phase partitioning in the model, and the bias will influence feedback processes in future climate simulations.

Data Availability Statement

The CloudSat data products were provided by the CloudSat Data Processing Center at CIRA/Colorado State University (https://www.cloudsat.cira.colostate.edu). CALIPSO-GOCCP data set version 3.1.2 was obtained from the ClimServ data center (https://climserv.ipsl.polytechnique.fr/cfmip-obs/Calipso_goccp.html). COSP is available online (https://github.com/CFMIP/COSPv2.0). The MIROC6 simulation data are available at https://doi.org/10.5281/zenodo.5977099.

Acknowledgments
The authors thank Gregory Cesana for helping to update the LiDAR simulator. The new microphysics and radiation schemes were optimized by Koji Ogochi. This research was supported by the Japan Society for the Promotion of Science KAKENHI (Grants JP19K14795 and JP19H05669); the Integrated Research Program for Advancing Climate Models (TOUGOU) and the Advanced Studies of Climate Change Projection (SENTAN) of the Ministry of Education, Culture, Sports, Science, and Technology (Grants JPMXD0717935457 and JPMXD0722680395); the Environment Research and Technology Development Fund (Grants JPMEERF20202R03 and JPMEERF21S12004) of the Environmental Restoration and Conservation Agency Provided by the Ministry of Environment of Japan; and the JST FOREST Program (Grant JPMJFR206Y). Simulations by MIROC-SPRINTARS were executed with the SX-Aurora TSUBASA supercomputer system of the National Institute for Environmental Studies, Japan. The authors thank three anonymous reviewers for providing valuable comments and suggestions that improved the manuscript.

References

Ackerman, S. A., Strabala, K. I., Menzel, W. P., Frey, R. A., Moeller, C. C., & Gumley, L. E. (1998). Discriminating clear sky from clouds with MODIS. *Journal of Geophysical Research: Atmospheres*, *103*(D24), 32141–32157. https://doi.org/10.1029/1998JD200032

Avramov, A., & Harrington, J. Y. (2010). Influence of parameterized ice habit on simulated mixed-phase Arctic clouds. *Journal of Geophysical Research*, *115*(D3), 1–14. https://doi.org/10.1029/2009jd012108

Bergeron, T. (1935). On the physics of cloud and precipitation. In *Proceeding 5th Assembly U.G.G.I. Lisbon* (Vol. *2*, p. 156).

Bintanja, R., & Selten, F. M. (2014). Future increases in Arctic precipitation linked to local evaporation and sea-ice retreat. *Nature*, *509*(7501), 479–482. https://doi.org/10.1038/nature13259

Bodas-Salcedo, A., Webb, M. J., Bony, S., Chepfer, H., Dufresne, J. L., Klein, S. A., et al. (2011). COSP: Satellite simulation software for model assessment. *Bulletin of the American Meteorological Society*, *92*(8), 1023–1043. https://doi.org/10.1175/2011BAMS2856.1

Boisvert, L. N., & Stroeve, J. C. (2015). The Arctic is becoming warmer and wetter as revealed by the Atmospheric Infrared Sounder. *Geophysical Research Letters*, *42*, 4439–4446. https://doi.org/10.1002/2015GL063775

Cesana, G., Ackerman, A., Fridlind, A., Silber, I., & Kelley, M. (2021). Snow reconciles observed and simulated phase partitioning and increases cloud feedback. *Geophysical Research Letters*, *48*(20), 1–11. https://doi.org/10.1029/2021GL094876

Cesana, G., & Chepfer, H. (2013). Evaluation of the cloud thermodynamic phase in a climate model using CALIPSO-GOCCP. *Journal of Geophysical Research: Atmospheres*, *118*(14), 7922–7937. https://doi.org/10.1002/jgrd.50376

Cesana, G., Del Genio, D. A., Ackerman, S. A., Kelley, M., Elsaesser, G., Fridlind, M. A., et al. (2019). Evaluating models response of tropical low clouds to SST forcings using CALIPSO observations. *Atmospheric Chemistry and Physics*, *19*(5), 2813–2832. https://doi.org/10.5194/acp-19-2813-2019

Cesana, G., Kay, J. E., Chepfer, H., English, J. M., & De Boer, G. (2012). Ubiquitous low-level liquid-containing Arctic clouds: New observations and climate model constraints from CALIPSO-GOCCP. *Geophysical Research Letters*, *39*(20), 1–6. https://doi.org/10.1029/2012GL053385

Cesana, G., Waliser, D. E., Jiang, X., & Li, J. F. (2015). Multimodel evaluation of cloud phase transition using satellite and reanalysis data. *Journal of Geophysical Research: Atmospheres*, *120*, 7871–7892. https://doi.org/10.1002/2014JD022932

Chepfer, H., Bony, S., Winker, D., Cesana, G., Dufresne, J. L., Minnis, P., et al. (2010). The GCM-oriented CALIPSO cloud product (CALIPSO-GOCCP). *Journal of Geophysical Research: Atmospheres*, *115*(5), 1–13. https://doi.org/10.1029/2009JD012251

Chepfer, H., Bony, S., Winker, D., Chiriaco, M., Dufresne, J. L., & Sèze, G. (2008). Use of CALIPSO lidar observations to evaluate the cloudiness simulated by a climate model. *Geophysical Research Letters*, *35*(15). https://doi.org/10.1029/2008GL034207

Cohen, J., Ye, H., & Jones, J. (2015). Trends and variability in rain-on-snow events. *Geophysical Research Letters*, *42*(17), 7115–7122. https://doi.org/10.1002/2015GL065320

Collins, M., Knutti, R., Arblaster, J., Dufresne, J.-L., Fichefet, T., Friedlingstein, P., et al. (2013). Long-term climate change: Projections, commitments and irreversibility. In *Climate change 2013: The physical science basis: Working Group I Contribution to the Fifth Assessment Report of the Intergovernmental Panel on Climate Change* (pp. 1029–1136).

Coopman, Q., Riedi, J., Finch, D. P., & Garrett, T. J. (2018). Evidence for changes in Arctic cloud phase due to long-range pollution transport. *Geophysical Research Letters*, *45*(19), 10709–10718. https://doi.org/10.1029/2018GL079873

Deng, M., MacE, G. G., Wang, Z., & Okamoto, H. (2010). Tropical composition, cloud, and climate coupling experiment validation for cirrus cloud profiling retrieval using cloudSat radar and CALIPSO lidar. *Journal of Geophysical Research: Atmospheres*, *115*(17), 1–18. https://doi.org/10.1029/2009JD013104

Eidhammer, T., Morrison, H., Bansemer, A., Gettelman, A., & Heymsfield, A. J. (2014). Comparison of ice cloud properties simulated by the Community Atmosphere Model (CAM5) with in situ observations. *Atmospheric Chemistry and Physics*, *14*(18), 10103–10118. https://doi.org/10.5194/acp-14-10103-2014

Eirund, G. K., Possner, A., & Lohmann, U. (2019). Response of Arctic mixed-phase clouds to aerosol perturbations under different surface forcings. *Atmospheric Chemistry and Physics*, *19*(15), 9847–9864. https://doi.org/10.5194/acp-19-9847-2019

Eliasson, S., Buehler, S. A., Milz, M., Eriksson, P., & John, V. O. (2011). Assessing observed and modeled spatial distributions of ice water path using satellite data. *Atmospheric Chemistry and Physics*, *11*(1), 375–391. https://doi.org/10.5194/acp-11-375-2011

English, J. M., Gettelman, A., & Henderson, G. R. (2015). Arctic radiative fluxes: Present-day biases and future projections in CMIP5 models. *Journal of Climate*, *28*(15), 6019–6038. https://doi.org/10.1175/JCLI-D-14-00801.1

Ervens, B., Feingold, G., Sulia, K., & Harrington, J. (2011). The impact of microphysical parameters, ice nucleation mode, and habit growth on the ice/liquid partitioning in mixed-phase Arctic clouds. *Journal of Geophysical Research: Atmospheres*, *116*(17). https://doi.org/10.1029/2011JD015729

Feist, M. M., Westbrook, C. D., Clark, P. A., Stein, T. H., Lean, H. W., & Stirling, A. J. (2019). Statistics of convective cloud turbulence from a comprehensive turbulence retrieval method for radar observations. *Quarterly Journal of the Royal Meteorological Society*, *145*(719), 727–744. https://doi.org/10.1002/qj.3462

Findeisen, W. (1938). Die Kolloidmeteorologischen Vorgange bei der Niederschlasbildung (collodial meteorological processes in the formation of precipitation). *Meteorologische Zeitschrift*, *55*, 121.

Forbes, R. M., & Ahlgrimm, M. (2014). On the representation of high-latitude boundary layer mixed-phase cloud in the ECMWF global model. *Monthly Weather Review*, *142*(9), 3425–3445. https://doi.org/10.1175/MWR-D-13-00325.1

Frey, W. R., & Kay, J. E. (2018). The influence of extratropical cloud phase and amount feedbacks on climate sensitivity. *Climate Dynamics*, *50*(7–8), 3097–3116. https://doi.org/10.1007/s00382-017-3796-5

Gettelman, A., Hannay, C., Bacmeister, J. T., Neale, R. B., Pendergrass, A. G., Danabasoglu, G., et al. (2019). High Climate Sensitivity in the Community Earth System Model version 2 (CESM2). *Geophysical Research Letters*, *46*(14), 8329–8337. https://doi.org/10.1029/2019GL083978

Gettelman, A., Morrison, H., Santos, S., Bogenschutz, P., & Caldwell, P. M. (2015). Advanced two-moment bulk microphysics for global models. Part II: Global model solutions and aerosol-cloud interactions. *Journal of Climate*, *28*(3), 1288–1307. https://doi.org/10.1175/JCLI-D-14-00103.1

Gettelman, A., Morrison, H., Terai, C. R., & Wood, R. (2013). Microphysical process rates and global aerosol-cloud interactions. *Atmospheric Chemistry and Physics*, *13*(19), 9855–9867. https://doi.org/10.5194/acp-13-9855-2013

Gettelman, A., Morrison, H., Thayer-Calder, K., & Zarzycki, C. M. (2019). The impact of rimed ice hydrometeors on global and regional climate. *Journal of Advances in Modeling Earth Systems*, *11*(6), 1543–1562. https://doi.org/10.1029/2018MS001488

Ghan, S. J., & Easter, R. C. (1992). Computationally efficient approximations to stratiform cloud microphysics parameterization. *Monthly Weather Review*, *120*, 1572–1582. https://doi.org/10.1175/1520-0493(1992)120<1572:ceatsc>2.0.co;2

Gierens, R., Kneifel, S., Shupe, M. D., Ebell, K., Maturilli, M., & Löhnert, U. (2020). Low-level mixed-phase clouds in a complex Arctic environment. *Atmospheric Chemistry and Physics*, *20*(6), 3459–3481. https://doi.org/10.5194/acp-20-3459-2020

Goosse, H., Kay, J. E., Armour, K. C., Bodas-Salcedo, A., Chepfer, H., Docquier, D., et al. (2018). Quantifying climate feedbacks in polar regions. *Nature Communications*, *9*(1), 1919. https://doi.org/10.1038/s41467-018-04173-0

Griesche, H. J., Ohneiser, K., Seifert, P., Radenz, M., Engelmann, R., & Ansmann, A. (2021). Contrasting ice formation in Arctic clouds: Surface-coupled vs. surface-decoupled clouds. *Atmospheric Chemistry and Physics*, *21*(13), 10357–10374. https://doi.org/10.5194/acp-21-10357-2021

Hartmann, D. L., & Short, D. A. (1980). On the use of Earth radiation budget statistics for studies of clouds and climate. *Journal of the Atmospheric Sciences*, *37*(6), 1233–1250. https://doi.org/10.1175/1520-0469(1980)037<1233:otuoer>2.0.co;2

Haynes, J. M., L'Ecuyer, T. S., Stephens, G. L., Miller, S. D., Mitrescu, C., Wood, N. B., & Tanelli, S. (2009). Rainfall retrieval over the ocean with spaceborne W-band radar. *Journal of Geophysical Research: Atmospheres*, *114*(8). https://doi.org/10.1029/2008JD009973

Haynes, J. M., Marchand, R. T., Luo, Z., Bodas-Salcedo, A., & Stephens, G. L. (2007). A multipurpose radar simulation package: QuickBeam. *Bulletin of the American Meteorological Society*, *88*(11), 1723–1728. https://doi.org/10.1175/BAMS-88-11-1723

Hill, P. G., Chiu, J. C., Allan, R. P., & Chern, J. D. (2018). Characterizing the radiative effect of rain using a global ensemble of cloud resolving simulations. *Journal of Advances in Modeling Earth Systems*, *10*(10), 2453–2470. https://doi.org/10.1029/2018MS001415

Hirota, N., Michibata, T., Shiogama, H., Ogura, T., & Suzuki, K. (2022). Impacts of precipitation modeling on cloud feedback in MIROC6. *Geophysical Research Letters*, *49*(5), 6–13. https://doi.org/10.1029/2021GL096523

Hogan, R. J., Francis, P., Flentje, H., Illingworth, A., Quante, M., & Pelon, J. (2003). Characteristics of mixed-phase clouds. Part I: Lidar, radar, and aircraft observations from CLARE '98. *Quarterly Journal of the Royal Meteorological Society*, *129*, 2089–2116. https://doi.org/10.1256/rj.01.208

Ingram, W., & Bushell, A. C. (2021). Sensitivity of climate feedbacks to vertical resolution in a general circulation model. *Geophysical Research Letters*, *48*(12), 1–9. https://doi.org/10.1029/2020GL092268

Jennings, K. S., Winchell, T. S., Livneh, B., & Molotch, N. P. (2018). Spatial variation of the rain-snow temperature threshold across the Northern Hemisphere. *Nature Communications*, *9*(1), 1–9. https://doi.org/10.1038/s41467-018-03629-7

Jing, X., Suzuki, K., & Michibata, T. (2019). The key role of warm rain parameterization in determining the aerosol indirect effect in a global climate model. *Journal of Climate*, *32*(14), 4409–4430. https://doi.org/10.1175/JCLI-D-18-0789.1

Kattsov, V. M., Walsh, J. E., Chapman, W. L., Govorkova, V. A., Pavlova, T. V., & Zhang, X. (2007). Simulation and projection of Arctic freshwater budget components by the IPCC AR4 global climate models. *Journal of Hydrometeorology*, *8*(3), 571–589. https://doi.org/10.1175/JHM575.1

Kay, J. E., Hillman, B. R., Klein, S. A., Zhang, Y., Medeiros, B., Pincus, R., et al. (2012). Exposing global cloud biases in the Community Atmosphere Model (CAM) using satellite observations and their corresponding instrument simulators. *Journal of Climate*, *25*(15), 5190–5207. https://doi.org/10.1175/JCLI-D-11-00469.1

Kay, J. E., L'Ecuyer, T., Pendergrass, A., Chepfer, H., Guzman, R., & Yettella, V. (2018). Scale-aware and definition-aware evaluation of modeled near-surface precipitation frequency using CloudSat observations. *Journal of Geophysical Research: Atmospheres*, *123*(8), 4294–4309. https://doi.org/10.1002/2017JD028213

Khairoutdinov, M., & Kogan, Y. (2000). A new cloud physics parameterization in a large-eddy simulation model of marine stratocumulus. *Monthly Weather Review*, *128*(1), 229–243. https://doi.org/10.1175/1520-0493(2000)128<0229:ancppi>2.0.co;2

King, M. D., Kaufman, Y. J., Menzel, W. P., & Tanre, D. (1992). Remote sensing of cloud, aerosol, and water vapor properties from the Moderate Resolution Imaging Spectrometer (MODIS). *IEEE Transactions on Geoscience and Remote Sensing*, *30*(1), 2–27. https://doi.org/10.1109/36.124212

Klein, S. A., & Jakob, C. (1999). Validation and sensitivities of frontal clouds simulated by the ECMWF model. *Monthly Weather Review*, *127*(10), 2514–2531. https://doi.org/10.1175/1520-0493(1999)127<2514:vasofc>2.0.co;2

Konsta, D., Dufresne, J. L., Chepfer, H., Idelkadi, A., & Cesana, G. (2016). Use of A-train satellite observations (CALIPSO-PARASOL) to evaluate tropical cloud properties in the LMDZ5 GCM. *Climate Dynamics*, *47*, 1263–1284. https://doi.org/10.1007/s00382-015-2900-y

Korolev, A., & Field, P. R. (2008). The effect of dynamics on mixed-phase clouds: Theoretical considerations. *Journal of the Atmospheric Sciences*, *65*(1), 66–86. https://doi.org/10.1175/2007JAS2355.1

Kubar, T. L., Hartmann, D. L., & Wood, R. (2009). Understanding the importance of microphysics and macrophysics for warm rain in marine low clouds. Part I: Satellite observations. *Journal of the Atmospheric Sciences*, *66*(10), 2953–2972. https://doi.org/10.1175/2009JAS3071.1

Lawson, R. P., & Gettelman, A. (2014). Impact of Antarctic mixed-phase clouds on climate. *Proceedings of the National Academy of Sciences of the United States of America*, *111*(51), 18156–18161. https://doi.org/10.1073/pnas.1418197111

Lenaerts, J. T., Drew Camron, M., Wyburn-Powell, C. R., & Kay, J. E. (2020). Present-day and future Greenland ice sheet precipitation frequency from CloudSat observations and the Community Earth System Model. *The Cryosphere*, *14*(7), 2253–2265. https://doi.org/10.5194/tc-14-2253-2020

Lenaerts, J. T., Gettelman, A., Van Tricht, K., van Kampenhout, L., & Miller, N. B. (2020). Impact of cloud physics on the Greenland ice sheet near-surface climate: A study with the community atmosphere model. *Journal of Geophysical Research: Atmospheres*, *125*(7). https://doi.org/10.1029/2019JD031470

Li, J. L. F., Richardson, M., Lee, W. L., Fetzer, E., Stephens, G., Jiang, J., et al. (2019). Potential faster Arctic sea ice retreat triggered by snowflakes' greenhouse effect. *The Cryosphere*, *13*(3), 969–980. https://doi.org/10.5194/tc-13-969-2019

Li, J. L. F., Xu, K. M., Jiang, J. H., Lee, W. L., Wang, L. C., Yu, J. Y., et al. (2020). An overview of CMIP5 and CMIP6 simulated cloud ice, radiation fields, surface wind stress, sea surface temperatures, and precipitation over tropical and subtropical oceans. *Journal of Geophysical Research: Atmospheres*, *125*(15), 5–10. https://doi.org/10.1029/2020JD032848

Mace, G. G., & Zhang, Q. (2014). The CloudSat radar-lidar geometrical profile product (RL-GeoProf): Updates, improvements, and selected results. *Journal of Geophysical Research: Atmospheres*, *119*, 9441–9462. https://doi.org/10.1002/2013JD021374

Marchand, R., & Ackerman, T. (2010). An analysis of cloud cover in multiscale modeling framework global climate model simulations using 4 and 1 km horizontal grids. *Journal of Geophysical Research: Atmospheres*, *115*(16), 1–19. https://doi.org/10.1029/2009JD013423

Marchand, R., Mace, G. G., Ackerman, T., & Stephens, G. (2008). Hydrometeor detection using Cloudsat—An Earth-orbiting 94 GHz cloud radar. *Journal of Atmospheric and Oceanic Technology*, *25*(4), 519–533. https://doi.org/10.1175/2007JTECHA1006.1

Matus, A. V., & L'Ecuyer, T. S. (2017). The role of cloud phase in Earth's radiation budget. *Journal of Geophysical Research*, *122*(5), 2559–2578. https://doi.org/10.1002/2016JD025951

McCoy, D. T., Tan, I., Hartmann, D. L., Zelinka, M. D., & Storelvmo, T. (2016). On the relationships among cloud cover, mixed-phase partitioning, and planetary albedo in GCMs. *Journal of Advances in Modeling Earth Systems*, *8*, 650–668. https://doi.org/10.1002/2015MS000589

McIlhattan, E. A., Kay, J. E., & L'Ecuyer, T. S. (2020). Arctic clouds and precipitation in the community Earth System Model version 2. *Journal of Geophysical Research: Atmospheres*, *125*(22), e2020JD032521. https://doi.org/10.1029/2020JD032521

McIlhattan, E. A., L'Ecuyer, T. S., & Miller, N. B. (2017). Observational evidence linking arctic supercooled liquid cloud biases in CESM to snowfall processes. *Journal of Climate*, *30*, 4477–4495. https://doi.org/10.1175/JCLI-D-16-0666.1

Michibata, T. (2022). Aerosol-cloud interactions in the climate system. In H. Akimoto, & H. Tanimoto (Eds.), *Springer handbook* (pp. 1–42). Springer Singapore. https://doi.org/10.1007/978-981-15-2527-8_35-3

Michibata, T., & Suzuki, K. (2020). Reconciling compensating errors between precipitation constraints and the energy budget in a climate model. *Geophysical Research Letters*, *47*(12), e2020GL088340. https://doi.org/10.1029/2020GL088340

Michibata, T., Suzuki, K., Ogura, T., & Jing, X. (2019). Incorporation of inline warm rain diagnostics into the COSP2 satellite simulator for process-oriented model evaluation. *Geoscientific Model Development*, *12*(10), 4297–4307. https://doi.org/10.5194/gmd-12-4297-2019

Michibata, T., Suzuki, K., Sato, Y., & Takemura, T. (2016). The source of discrepancies in aerosol-cloud-precipitation interactions between GCM and A-Train retrievals. *Atmospheric Chemistry and Physics*, *16*(23), 15413–15424. https://doi.org/10.5194/acp-16-15413-2016

Michibata, T., Suzuki, K., Sekiguchi, M., & Takemura, T. (2019). Prognostic precipitation in the MIROC6-SPRINTARS GCM: Description and evaluation against satellite observations. *Journal of Advances in Modeling Earth Systems*, *11*(3), 839–860. https://doi.org/10.1029/2018MS001596

Michibata, T., Suzuki, K., & Takemura, T. (2020). Snow-induced buffering in aerosol-cloud interactions. *Atmospheric Chemistry and Physics*, *20*(22), 13771–13780. https://doi.org/10.5194/acp-20-13771-2020

Milbrandt, J. A., & Morrison, H. (2016). Parameterization of cloud microphysics based on the prediction of bulk ice particle properties. Part III: Introduction of multiple free categories. *Journal of the Atmospheric Sciences*, *73*(3), 975–995. https://doi.org/10.1175/JAS-D-15-0204.1

Mitchell, J. F. B., Senior, C. A., & Ingram, W. J. (1989). CO_2 and climate: A missing feedback? *Nature*, *341*, 132–134. https://doi.org/10.1038/341132a0

Morrison, H., De Boer, G., Feingold, G., Harrington, J., Shupe, M. D., & Sulia, K. (2012). Resilience of persistent Arctic mixed-phase clouds. *Nature Geoscience*, *5*(1), 11–17. https://doi.org/10.1038/ngeo1332

Morrison, H., & Gettelman, A. (2008). A new two-moment bulk stratiform cloud microphysics scheme in the community atmosphere model, version 3 (CAM3). Part I: Description and numerical tests. *Journal of Climate*, *21*(15), 3642–3659. https://doi.org/10.1175/2008JCLI2105.1

Morrison, H., McCoy, R., Klein, S., Xie, S., Luo, Y., Avramov, A., et al. (2009). Intercomparison of model simulations of mixed-phase clouds observed during the ARM Mixed-Phase Arctic Cloud Experiment. II: Multilayer cloud. *Quarterly Journal of the Royal Meteorological Society*, *135*(641), 1003–1019. https://doi.org/10.1002/qj.415

Mülmenstädt, J., Salzmann, M., Kay, J. E., Zelinka, M. D., Ma, P. L., Nam, C., et al. (2021). An underestimated negative cloud feedback from cloud lifetime changes. *Nature Climate Change*, *11*(6), 508–513. https://doi.org/10.1038/s41558-021-01038-1

Mülmenstädt, J., Sourdeval, O., Delanoë, J., & Quaas, J. (2015). Frequency of occurrence of rain from liquid-, mixed-, and ice-phase clouds derived from A-Train satellite retrievals. *Geophysical Research Letters*, *42*(15), 6502–6509. https://doi.org/10.1002/2015GL064604

Murray-Watson, R. J., & Gryspeerdt, E. (2022). Stability-dependent increases in liquid water with droplet number in the Arctic. *Atmospheric Chemistry and Physics*, *22*(9), 5743–5756. https://doi.org/10.5194/acp-22-5743-2022

Nakajima, T. Y., Suzuki, K., & Stephens, G. L. (2010). Droplet growth in warm water clouds observed by the A-train. Part II: A multisensor view. *Journal of the Atmospheric Sciences*, *67*(6), 1897–1907. https://doi.org/10.1175/2010JAS3276.1

Nam, C., Bony, S., Dufresne, J. L., & Chepfer, H. (2012). The too few, too bright tropical low-cloud problem in CMIP5 models. *Geophysical Research Letters*, *39*(21). https://doi.org/10.1029/2012GL053421

Perovich, D. K., Grenfell, T. C., Light, B., & Hobbs, P. V. (2002). Seasonal evolution of the albedo of multiyear Arctic sea ice. *Journal of Geophysical Research C: Oceans*, *107*(10), 1–13. https://doi.org/10.1029/2000jc000438

Pincus, R., Platnick, S., Ackerman, S. A., Hemler, R. S., & Patrick Hofmann, R. J. (2012). Reconciling simulated and observed views of clouds: MODIS, ISCCP, and the limits of instrument simulators. *Journal of Climate*, *25*(13), 4699–4720. https://doi.org/10.1175/JCLI-D-11-00267.1

Polonsky, I. N., Labonnote, L. C., & Cooper, S. (2008). Level 2 cloud optical depth product process description and interface control document. In *Paper presented at CloudSat Project: A NASA Earth System Science Pathfinder Mission*. CIRA/Colorado State University.

Posselt, R., & Lohmann, U. (2008). Introduction of prognostic rain in ECHAM5: Design and single column model simulations. *Atmospheric Chemistry and Physics*, *8*(11), 2949–2963. https://doi.org/10.5194/acp-8-2949-2008

Rasch, P. J., Xie, S., Ma, P. L., Lin, W., Wang, H., Tang, Q., et al. (2019). An overview of the atmospheric component of the energy Exascale Earth System Model. *Journal of Advances in Modeling Earth Systems*, *11*(8), 2377–2411. https://doi.org/10.1029/2019MS001629

Roehrig, R., Beau, I., Saint-Martin, D., Alias, A., Decharme, B., Guérémy, J. F., et al. (2020). The CNRM Global Atmosphere Model ARPEGE-Climat 6.3: Description and evaluation. *Journal of Advances in Modeling Earth Systems*, *12*(7), 1–53. https://doi.org/10.1029/2020MS002075

Sant, V., Posselt, R., & Lohmann, U. (2015). Prognostic precipitation with three liquid water classes in the ECHAM5-HAM GCM. *Atmospheric Chemistry and Physics*, *15*(15), 8717–8738. https://doi.org/10.5194/acp-15-8717-2015

Schär, C., Lüthi, D., Beyerle, U., & Heise, E. (1999). The soil-precipitation feedback: A process study with a regional climate model. *Journal of Climate*, *12*(2–3), 722–741. https://doi.org/10.1175/1520-0442(1999)012<0722:tspfap>2.0.co;2check doi

Screen, J. A., & Simmonds, I. (2010). The central role of diminishing sea ice in recent Arctic temperature amplification. *Nature*, *464*(7293), 1334–1337. https://doi.org/10.1038/nature09051

Serreze, M. C., Barrett, A. P., Stroeve, J. C., Kindig, D. N., & Holland, M. M. (2009). The emergence of surface-based Arctic amplification. *The Cryosphere*, *3*(1), 11–19. https://doi.org/10.5194/tc-3-11-2009

Shupe, M. D., Turner, D. D., Walden, V. P., Bennartz, R., Cadeddu, M. P., Castellani, B. B., et al. (2013). High and dry: New observations of tropospheric and cloud properties above the Greenland ice sheet. *Bulletin of the American Meteorological Society*, *94*(2), 169–186. https://doi.org/10.1175/BAMS-D-11-00249.1

Smalley, M., L'Ecuyer, T., Lebsock, M., & Haynes, J. (2014). A comparison of precipitation occurrence from the NCEP StageIV QPE Product and the CloudSat Cloud Profiling Radar. *Journal of Hydrometeorology*, *15*(1), 444–458. https://doi.org/10.1175/JHM-D-13-048.1

Stephens, G. L., L'Ecuyer, T., Forbes, R., Gettlemen, A., Golaz, J. C., Bodas-Salcedo, A., et al. (2010). Dreary state of precipitation in global models. *Journal of Geophysical Research: Atmospheres*, *115*(24). https://doi.org/10.1029/2010JD014532

Stephens, G. L., Vane, D. G., Boain, R. J., Mace, G. G., Sassen, K., & Wang, Z. (2002). The CloudSat mission and the A-train: A new dimension of space-based observations of clouds and precipitation. *Bulletin of the American Meteorological Society*, *83*(12), 1771–1790. https://doi.org/10.1175/BAMS-83-12-1771

Stephens, G. L., Vane, D. G., Tanelli, S., Im, E., Durden, S., Rokey, M., et al. (2008). CloudSat mission: Performance and early science after the first year of operation. *Journal of Geophysical Research: Atmospheres*, *114*(8), 1–18. https://doi.org/10.1029/2008JD009982

Sturm, M., Holmgren, J., & Perovich, D. K. (2002). Winter snow cover on the sea ice of the Arctic Ocean at the Surface Heat Budget of the Arctic Ocean (SHEBA): Temporal evolution and spatial variability. *Journal of Geophysical Research: Oceans*, *107*(10), 1–17. https://doi.org/10.1029/2000jc000400

Suzuki, K., Stephens, G., Bodas-Salcedo, A., Wang, M., Golaz, J. C., Yokohata, T., & Koshiro, T. (2015). Evaluation of the warm rain formation process in global models with satellite observations. *Journal of the Atmospheric Sciences*, *72*(10), 3996–4014. https://doi.org/10.1175/JAS-D-14-0265.1

Suzuki, K., & Stephens, G. L. (2008). Global identification of warm cloud microphysical processes with combined use of A-Train observations. *Geophysical Research Letters*, *35*(8), 1–5. https://doi.org/10.1029/2008GL033590

Swales, D. J., Pincus, R., & Bodas-Salcedo, A. (2018). The cloud feedback model Intercomparison Project Observational Simulator Package: Version 2. *Geoscientific Model Development*, *11*(1), 77–81. https://doi.org/10.5194/gmd-11-77-2018

Takemura, T., Egashira, M., Matsuzawa, K., Ichijo, H., O'Ishi, R., & Abe-Ouchi, A. (2009). A simulation of the global distribution and radiative forcing of soil dust aerosols at the Last Glacial Maximum. *Atmospheric Chemistry and Physics*, *9*(9), 3061–3073. https://doi.org/10.5194/acp-9-3061-2009

Takemura, T., Nakajima, T., Dubovik, O., Holben, B. N., & Kinne, S. (2002). Single-scattering albedo and radiative forcing of various aerosol species with a global three-dimensional model. *Journal of Climate*, *15*(4), 333–352. https://doi.org/10.1175/1520-0442(2002)015<0333:ssaarf>2.0.co;2

Takemura, T., Nozawa, T., Emori, S., Nakajima, T. Y., & Nakajima, T. (2005). Simulation of climate response to aerosol direct and indirect effects with aerosol transport-radiation model. *Journal of Geophysical Research D: Atmospheres*, *110*(2), 1–16. https://doi.org/10.1029/2004JD005029

Takemura, T., Okamoto, H., Maruyama, Y., Numaguti, A., Higurashi, A., & Nakajima, T. (2000). Global three-dimensional simulation of aerosol optical thickness distribution of various origins. *Journal of Geophysical Research*, *105*, 17853–17873. https://doi.org/10.1029/2000JD900265

Tan, I., Storelvmo, T., & Zelinka, M. D. (2016). Observational constraints on mixed-phase clouds imply higher climate sensitivity. *Science*, *352*, 224–227. https://doi.org/10.1126/science.aad5300

Tanelli, S., Durden, S. L., Im, E., Pak, K. S., Reinke, D. G., Partain, P., et al. (2008). CloudSat's cloud profiling radar after two years in orbit: Performance, calibration, and processing. *IEEE Transactions on Geoscience and Remote Sensing*, *46*(11), 3560–3573. https://doi.org/10.1109/TGRS.2008.2002030

Tatebe, H., Ogura, T., Nitta, T., Komuro, Y., Ogochi, K., Takemura, T., et al. (2019). Description and basic evaluation of simulated mean state, internal variability, and climate sensitivity in MIROC6. *Geoscientific Model Development*, 1–92. https://doi.org/10.5194/gmd-2018-155

Walters, D., Baran, A. J., Boutle, I., Brooks, M., Earnshaw, P., Edwards, J., et al. (2019). The Met Office Unified Model Global Atmosphere 7.0/7.1 and JULES Global Land 7.0 configurations. *Geoscientific Model Development*, *12*(5), 1909–1963. https://doi.org/10.5194/gmd-12-1909-2019

Walters, D. N., Best, M. J., Bushell, A. C., Copsey, D., Edwards, J. M., Falloon, P. D., et al. (2011). The Met Office Unified Model Global Atmosphere 3.0/3.1 and JULES Global Land 3.0/3.1 configurations. *Geoscientific Model Development*, *4*(4), 919–941. https://doi.org/10.5194/gmd-4-919-2011

Wang, C., Soden, B. J., Yang, W., & Vecchi, G. A. (2021). Compensation between cloud feedback and aerosol-cloud interaction in CMIP6 models. *Geophysical Research Letters*, *48*(4), 1–10. https://doi.org/10.1029/2020GL091024

Watanabe, M., Emori, S., Satoh, M., & Miura, H. (2009). A PDF-based hybrid prognostic cloud scheme for general circulation models. *Climate Dynamics*, *33*(6), 795–816. https://doi.org/10.1007/s00382-008-0489-0

Webb, M., Senior, C., Bony, S., & Morcrette, J. J. (2001). Combining ERBE and ISCCP data to assess clouds in the Hadley Centre, ECMWF, and LMD atmospheric climate models. *Climate Dynamics*, *17*(12), 905–922. https://doi.org/10.1007/s003820100157

Wilson, D. R., & Ballard, S. P. (1999). A microphysically based precipitation scheme for the UK Meteorological Office unified model. *Quarterly Journal of the Royal Meteorological Society*, *125*, 1607–1636. https://doi.org/10.1002/qj.49712555707

Winker, D. M., Tackett, J. L., Getzewich, B. J., Liu, Z., Vaughan, M. A., & Rogers, R. R. (2013). The global 3-D distribution of tropospheric aerosols as characterized by CALIOP. *Atmospheric Chemistry and Physics*, *13*(6), 3345–3361. https://doi.org/10.5194/acp-13-3345-2013

Winker, D. M., Vaughan, M. A., Omar, A., Hu, Y., Powell, K. A., Liu, Z., et al. (2009). Overview of the CALIPSO mission and CALIOP data processing algorithms. *Journal of Atmospheric and Oceanic Technology*, *26*(11), 2310–2323. https://doi.org/10.1175/2009JTECHA1281.1

Wood, N. B., L'Ecuyer, T. S., Heymsfield, A. J., Stephen, G. L., Hudak, D. R., & Rodriguez, P. (2014). Estimating snow microphysical properties using collocated multisensor observations. *Journal of Geophysical Research*, *119*(14), 8941–8961. https://doi.org/10.1002/2013JD021303

Wood, N. B., L'Ecuyer, T. S., Vane, D., Stephens, G. L., & Partain, P. (2013). *Level 2C snow profile process description and interface control document* (p. 21). JPL Doc.

You, Y., Peters-Lidard, C., Ringerud, S., & Haynes, J. M. (2021). Evaluation of rainfall-snowfall separation performance in remote sensing data sets. *Geophysical Research Letters*, *48*(21), 1–10. https://doi.org/10.1029/2021gl094180

Zamora, L. M., Kahn, R. A., Huebert, K. B., Stohl, A., & Eckhardt, S. (2018). A satellite-based estimate of combustion aerosol cloud microphysical effects over the Arctic Ocean. *Atmospheric Chemistry and Physics*, *18*(20), 14950–14964. https://doi.org/10.5194/acp-18-14949-2018

Zelinka, M. D., Klein, S. A., Qin, Y., & Myers, T. A. (2022). Evaluating climate models' cloud feedbacks against expert judgment. *Journal of Geophysical Research: Atmospheres*, *127*(2), 1–18. https://doi.org/10.1029/2021JD035198

Zelinka, M. D., Myers, T. A., McCoy, D. T., Po-Chedley, S., Caldwell, P. M., Ceppi, P., et al. (2020). Causes of higher climate sensitivity in CMIP6 models. *Geophysical Research Letters*, *47*(1), 1–12. https://doi.org/10.1029/2019GL085782

Zhang, M., Liu, X., Diao, M., D'Alessandro, J. J., Wang, Y., Wu, C., et al. (2019). Impacts of representing heterogeneous distribution of cloud liquid and ice on phase partitioning of arctic mixed-phase clouds with NCAR CAM5. *Journal of Geophysical Research: Atmospheres*, *124*(23), 13071–13090. https://doi.org/10.1029/2019JD030502